Minimizing Paste Content in Concrete Using Limestone Powders – Demonstration Mixtures

TECHNICAL REPORT · JANUARY 2016

DOI: 10.6028/NIST.TN.1906

3 AUTHORS, INCLUDING:

D. P. Bentz

National Institute of Standards and Technolo…

331 PUBLICATIONS **6,771** CITATIONS

SEE PROFILE

Scott Zachary Jones

National Institute of Standards and Technolo…

10 PUBLICATIONS **14** CITATIONS

SEE PROFILE

NIST Technical Note 1906

Minimizing Paste Content in Concrete Using Limestone Powders – Demonstration Mixtures

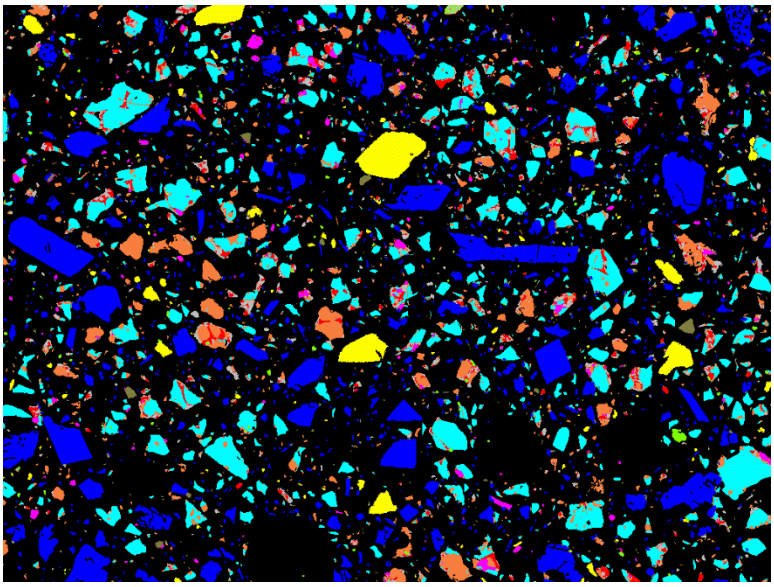

Dale P. Bentz
Scott Z. Jones
Didier Lootens

This publication is available free of charge from:
http://dx.doi.org/10.6028/NIST.TN.1906

National Institute of Standards and Technology
U.S. Department of Commerce

NIST Technical Note 1906

Minimizing Paste Content in Concrete Using Limestone Powders – Demonstration Mixtures

Dale P. Bentz
Scott Z. Jones
Materials and Structural Systems Division
Engineering Laboratory

Didier Lootens
Sika Technology AG - Central Research

This publication is available free of charge from:
http://dx.doi.org/10.6028/NIST.TN.1906

January 2016

U.S. Department of Commerce
Penny Pritzker, Secretary

National Institute of Standards and Technology
Willie May, Under Secretary of Commerce for Standards and Technology and Director

National Institute of Standards and Technology Technical Note 1906
Natl. Inst. Stand. Technol. Tech. Note 1906, 38 pages (January 2016)
CODEN: NTNOEF

This publication is available free of charge from:
http://dx.doi.org/10.6028/NIST.TN.1906

Abstract

In recent years, there has been great interest in reducing the cement content of concrete, due to the high energy and carbon dioxide footprints of cement production. There are numerous (waste) materials that can be substituted for cement in the concrete mixture proportions, including fly ash, slag, silica fume, metakaolin, waste glass, etc. However, a more abundant material substitute would be limestone powder, created from the same limestone that is currently heavily employed in cement production as the primary source of calcium oxide. This technical note presents an approach to replacing not only cement powder, but effectively cement paste consisting of the cement and water, with appropriately sized limestone powder(s). Such an approach effectively extends the conventional utilization of centimeter-sized coarse aggregates (rocks) and millimeter-sized fine aggregates (sand) that occupy between 65 % and 75 % of the volume of a concrete structure to include micro-aggregates ranging between about 1 μm and 100 μm in size. Here, to demonstrate the feasibility of this approach, demonstration mixtures of pastes, mortars, and concretes are each formulated with limestone powder replacement for a significant portion of their cement paste component, achieving cement reductions of up to 28 % in concrete, for example. For these mixture modifications, the water-to-cement mass ratio (*w/c*) is maintained at or above 0.4 to provide sufficient water to react with all of the cement, so that none of this most costly component of cement-based materials goes to waste. Meanwhile, the water-to-solids ratio (*w/s*) is reduced to a value in the range of 0.22 to 0.40 in order to maximize the limestone powder replacement level, while still providing sufficient flow and rheology, by using reasonable dosages of high range water reducing admixtures. The fresh, early age, and long term performance properties of these high volume limestone powder (HVLP) mixtures are contrasted with a *w/c*=0.4 ordinary portland cement (OPC) paste or mortar, or a *w/c*=0.5 OPC concrete reference, respectively. In general, the properties and performance of these more sustainable mixtures are similar or even superior to those of the corresponding reference mixture, suggesting that these new paradigm HVLP concretes could be readily substituted for existing conventional OPC mixtures. The reduced shrinkage (autogenous and drying) of the mortars with limestone powder replacement, due to their reduced paste content, is highlighted because of its likelihood to reduce concrete cracking. However, beyond measurements of electrical resistivity, this study has not specifically focused on durability issues and additional research on this topic is recommended as these new mixtures are reduced to (field) practice.

Keywords: Concrete; high range water reducing admixture; high volume limestone powder; mortar; paste content; sustainability.

Table of Contents

List of Tables

List of Figures

Introduction

Over the years, extensive effort and discussion has been focused on optimal aggregate gradations for concrete [1], such as the 0.45 power law and the original Fuller curve (0.5 power law). One focus of these efforts is on increasing the volume fraction of (fine and coarse) aggregates in concrete from 60 % upwards to about 75 %, recognizing that a reduced paste content generally corresponds to reduced shrinkage and improved transport properties, since the aggregates are generally non-shrinking and relatively impermeable. Typically, in a 75 % aggregate volume fraction concrete, the remaining 25 % is occupied by cement paste and entrained air. For a water-cement by mass ratio, *w/c*=0.4, cement paste (such as exemplified in Figure 1 [2]), the volume fraction of the paste occupied by the water is about 56 %. If one had continued to apply the packing considerations being implemented at the aggregate level, a much lower water volume fraction within the paste (perhaps moving towards 35 % of the paste volume, equivalent to a *w/c* of about 0.17) would have been expected.

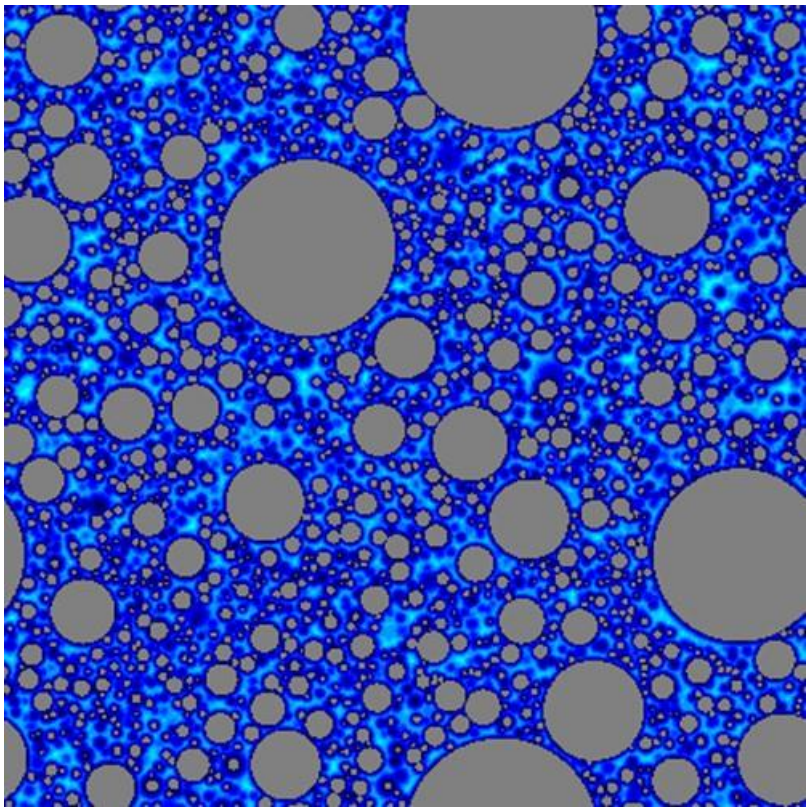

Figure 1. Two-dimensional slice from a three-dimensional model of spherical cement particles in water. Cement particles are grey and shades of blue indicate distances of water from the nearest cement particle surface, with lighter blues indicating a greater distance [2].

While it is well known that reducing the water content (and *w/c* concurrently) will increase strengths (e.g., Abram's law [3]) and reduce transport rates, it is only with the advent of water reducers and subsequent development of high-range water reducing admixtures (HRWRA) that the production of low *w/c* (or water-to-cementitious materials, *w/cm*) concretes have become

commonplace. However, below a *w/c* of about 0.42 for sealed conditions (0.36 for saturated curing), there is insufficient space (or water in the case of sealed curing) for all of the cement to hydrate and a portion remains unreacted as a rather expensive filler material [4]. While it has been previously suggested to replace this unreacted portion of the cement with a less expensive and greener material such as limestone powder [4,5], an alternative and perhaps more appropriate view is to consider the replacement of both cement and water (i.e., cement paste) with the limestone powder, producing a high volume limestone powder (HVLP) mixture. Such an approach has the potential to substantially reduce the carbon and energy footprints of the concrete and can also conserve a significant volume of water in drought-stricken regions of the world.

The recent results of Li and Kwan have quantitatively demonstrated the utility of these limestone fines concretes [6]. Here, as a further proof of this concept, results from demonstration mixtures for pastes, mortars, and concretes will be presented, with an ordinary portland cement (OPC) paste/mortar/concrete with a *w/c*=0.4 (0.5 for concrete) serving as a reference. While the limestone powder mixtures presented in this study are similar to some of the current mixtures being employed for self-consolidating concrete (SCC) applications (particularly in Europe), it is hoped that these results will spur the construction sector to consider such mixtures for a wider variety of applications, leading to significant reductions in the consumption of cement and water by the concrete industry, without reducing concrete production or sacrificing performance. The use of the limestone powder as the filler is particularly attractive in that the limestone particle surfaces serve as nucleation and growth sites for the products of cement hydration, accelerating and amplifying the early-age hydration reactions [7]. Additionally, the fine limestone particles, while much less reactive than cement, do react slightly within the cementitious system to form carboaluminate hydration products, including calcium hemicarboaluminate and calcium monocarboaluminate, while stabilizing the ettringite that is formed at early ages. Thus, the limestone particles are not "inert", but instead become an integral part and stabilizer of the percolated network of particles and hydration products that lead to setting and strength development in cement-based systems [7,8].

Materials and Methods

Materials

The portland cement used in the present study was an ASTM C150 Type I/II portland cement [9] with a 3.7 % limestone (91.0 % $CaCO_3$) addition. According to the mill test certificate reports provided by the manufacturer for various batches employed in this study, it has a Blaine fineness of 374 m^2/kg to 384 m^2/kg and an adjusted potential Bogue composition of 53.5 % to 58.9 % C_3S[1], 11.6 % to 16.2 % C_2S, 6.8 % to 7.4 % C_3A, and 9.5 % to 10.3 % C_4AF by mass. The density of the cement measured using helium pycnometry at NIST was 3164 kg/m^3 ± 2 kg/m^3. A series of limestone (> 95 % $CaCO_3$) powders obtained from a single manufacturer with median diameters of 1.6 µm, 2.2 µm, 4 µm, and 16 µm (as measured at NIST, see Figure 2) were employed in the initial paste studies. Additionally, two limestone powders with broader particle size distributions (PSDs) and median particle sizes of 6.7 µm and 19.2 µm, obtained from two other manufacturers, were employed in the later mortar and concrete studies. The 6.7 µm limestone powder was obtained from a local limestone crushing operation as the dust of fracture passing a #100 sieve (150 µm opening). Based on thermogravimetric analysis (TGA), its calcium carbonate content was estimated as 98.1 % ± 0.6 % (standard deviation for three replicates), assuming that only $CaCO_3$ is present in the dust and ignoring any $MgCO_3$ that may be present.

The measured BET (Brunauer-Emmett-Teller) surface area of the cement using nitrogen gas as the sorbent is 1.39 m^2/g, while the series of four limestone powders from the same manufacturer have surface areas of 9.93 m^2/g, 7.06 m^2/g, 2.42 m^2/g, and 0.83 m^2/g, respectively, as measured previously at NIST [10]. For the 2.2 µm median diameter powder, three replicate measurements indicated a standard deviation of 0.14 m^2/g in surface area. The measured surfaces areas for the 6.7 µm and 19.2 µm limestone powders were 1.54 m^2/g and 0.696 m^2/g, respectively, indicating a good ranking of limestone powder surface area according to median particle size. The density of the initial limestone powders was reported by their manufacturer to be 2710 kg/m^3, while those of the broad distribution 6.7 µm and 19.2 µm limestone powders were measured at NIST as 2740 kg/m^3 ± 10 kg/m^3 and 2760 kg/m^3 ± 10 kg/m^3, respectively. The measured PSDs of each of the seven powders (cement and six limestones) as obtained using laser diffraction [11] are provided in Figure 2.

Various polycarboxylate-based commercial HRWRA admixtures obtained from three different manufacturers were used to provide adequate flow/slump for the pastes, mortars, and concretes prepared with the cement/limestone powders blend. The *w/c*=0.4 control OPC paste and mortar specimens were prepared without any chemical admixtures, while the *w/c*=0.5 OPC concrete contained a dosage of 1.08 L/m^3 of one of the HRWRA.

Paste Studies

Initial studies focused on pastes in order to investigate the best combination of (two) limestones to utilize in subsequent mixtures, as well as their proportions. To produce a homogeneous and reproducible paste, samples were prepared using a (kitchen) mixer in a two-

[1] In conventional cement chemistry notation, C=CaO, S=SiO_2, A=Al_2O_3, and F=Fe_2O_3.

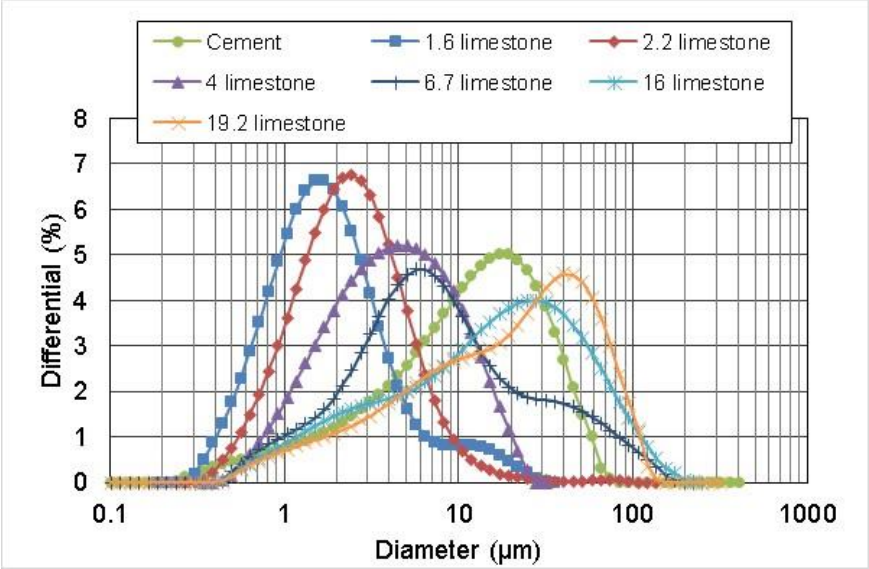

Figure 2. Measured particle size distributions for the cement and the six limestone powders. Each shown result is the average of six individual measurements and the error bars (one standard deviation) would fall within the size of the shown symbols.

stage mixing procedure in which approximately half of the water (with admixture HRWRA A) was added to the powder blend and mixed for 30 s on the lowest speed of the mixer. Next, the remainder of the liquid was added and mixing continued for another 30 s on the lowest speed. Following a scraping of the mixing bowl, mixing concluded with 60 s of mixing on the 2nd lowest speed of the mixer. The total preparation time of a paste was thus on the order of 3 min.

Pastes were characterized by their fresh temperature, rheology as measured using a parallel (serrated) plate rotational rheometer, isothermal calorimetry (ITC), and packing fraction via centrifuging of about 50 g of the prepared paste at 800 g for 3 min at 25 °C [12]. For the rheology measurements, the plates had a diameter of 35 mm, with a gap of 0.4 mm. A sweep in shear rate was performed on each mixture, with the resultant shear stress being recorded. For ITC, the average absolute difference between replicate specimens was previously measured to be 2.4×10^{-5} W/g (cement), for measurements conducted between 1 h and 7 d after mixing [13].

Mortar Studies

Following the paste studies, six mortar mixtures were examined; their mixture proportions are provided in Table 1. Each mortar was prepared using a blend of four sands to achieve a 55 % sand volume fraction (neglecting air entrapped in the mixture). For the lower water-to-solids mass ratio (*w/s*=0.25) mortars, cement/limestone powder mixtures were prepared both with a 10:90 blended mixture of the fine (2.2 µm) and coarse (16 µm) limestone powders and with just the coarser limestone. For the five mortars using a cement-limestone blend, all of the powder components were pre-mixed for 30 min using a three-dimensional laboratory mixer that simultaneously rolls and tumbles the (mixing) container. The *w/c*=0.4 OPC reference mortar was prepared without any chemical admixtures and mixed according to the documented ASTM Practice C305 procedures for mortars [9]. Meanwhile, a 5 mL/kg powder dosage of the liquid HRWRA was used in the *w/s*=0.25 and *w/s*=0.28 cement/limestone powder mortars, with an

Table 1. Mortar mixture proportions

	***w/c*=0.4 control**	***w/s*=0.25 LS blend**	***w/s*=0.25 16 µm LS**	***w/s*=0.28 LS blend**	***w/s*=0.30 6.7 µm LS**	***w/s*=0.30 19.2 µm LS**
Cement	1250 g	956.3 g	956.3 g	775.7 g	829.9 g	828.7 g
2.2 µm limestone	---	57.0 g	---	66.5 g	---	---
16 µm limestone	---	512.9 g	569.9 g	598.7 g	---	---
6.7 µm limestone	---	---	---	---	575.7 g	---
19.2 µm limestone	---	---	---	---	---	579.1 g
Water	500 g	381.6 g	381.6 g	403.4 g	421.7 g	422.3 g
F95 fine sand	712.5 g	713.2 g	713.2 g	713.3 g	713.3 g	713.3 g
C778 graded sand	541.5 g	542.0 g	542.0 g	542.1 g	542.1 g	542.1 g
C778 20-30 sand	541.5 g	542.0 g	542.0 g	542.1 g	542.1 g	542.1 g
S16 coarse sand	1054.5 g	1055.5 g	1055.5 g	1055.7 g	1055.6 g	1055.6 g
Polycarboxylate-based HRWRA (mL/kg powder)	---	5.0 mL/kg HRWRA B	5.0 mL/kg HRWRA B	5.0 mL/kg HRWRA B	3.17 mL/kg HRWRA D with 0.8 mL/kg HRWRA E	3.56 mL/kg HRWRA C
w/c	0.40	0.40	0.40	0.52	0.51	0.51
Cement reduction	---	23.5 %	23.5 %	37.9 %	33.6 %	33.7 %
Water reduction	---	23.5 %	23.5 %	19.3 %	15.7 %	15.5 %
Cement paste volume reduction	---	23.5 %	23.5 %	27.5 %	23.5 %	23.5 %

assumed solids content of 50 % for the HRWRA. For the two *w/s*=0.30 cement/limestone powder mortars, different HRWRAs were employed at the dosages indicated in Table 1. For these latter five mortars, about 2/3rd of the mixing water was added to the mixing bowl and blended with all of the powder for 30 s on low speed, prior to adding the remainder of the mixing water and all of the HRWRA dosage. This second water addition was followed by another 30 s of mixing on low speed. Next, the sand was added during 30 s of low speed mixing, followed by 1 min of medium speed mixing. Following a 1 min rest, the preparation concluded with 1 min of medium speed mixing. In an attempt to control the temperature of the prepared mortars, all materials were conditioned overnight and mixing was conducted inside an environmental chamber maintained at 21 °C ± 1°C, except for the *w/s*=0.28 mortar that was prepared under laboratory conditions (nominally 23 °C ± 2 °C).

The following measurements [9] were conducted on the prepared mortars: unit (cup) weight and air content (ASTM C185-08), temperature, flow table (ASTM C1437-13), Vicat needle penetration measurements (following ASTM C191-13), ITC (ASTM C1702-15) to 7 d, semi-adiabatic calorimetry to 3 d, compressive strength (cubes, per ASTM C109/C109M-13) at 1 d, 7 d, 28 d, and 91 d, autogenous shrinkage (ASTM C1698-09) to 28 d, and drying shrinkage (ASTM C596-09) to 28 d. For the semi-adiabatic calorimetry, replicate specimens have indicated a standard deviation of 1.4 °C in the maximum specimen temperature achieved during a 3 d test [14].

Concrete Mixtures

In the final stage of the current study, concrete mixtures were prepared with a batch size of 60 L in a rotating pan mixer with bottom discharge. Mixture proportions of the three concrete mixtures are provided in Table 2. As indicated in the table, the (volume) fractions of the fine and coarse aggregates were held constant in all mixtures with a total aggregate volume fraction of 70 %. The densities of the fine and coarse aggregates taken from their manufacturers' specifications were 2610 kg/m^3 and 2810 kg/m^3, respectively. The measured absorptions of the fine (silica concrete sand) and coarse (dolomitic limestone) aggregates were 1.1 % ± 0.1 % and 0.40 % ± 0.05 % by dry mass, respectively, and both were added to the concrete in an oven dry condition, with the mix water being adjusted (increased) accordingly. The particle size distributions of all dry materials used in the concrete mixtures are provided in Figure 3. A single HRWRA (HRWRA C) was utilized in all of the concrete mixtures (based on its previously observed minimal retardation of cement hydration).

The fresh concrete mixtures were characterized by measurements [15] of fresh concrete temperature (ASTM C1064, ± 0.1 °C), unit weight (ASTM C138, ± 10 kg/m^3) and calculated air content, and slump (ASTM C143, ± 10 mm). Concrete was sieved through a number 8 sieve (2.38 mm opening) to obtain mortar for ITC (about 7.5 g of mortar in a sealed vial) and setting measurements using both a Vicat needle (ASTM C191 protocol) and a mortar penetrometer (ASTM C403, ± 3.5 min for initial set and ± 4.4 min for final set). For each mixture, twenty 101.6 mm (4") diameter by 203.2 mm (8") length cylinders were cast, along with four 50.8 mm by 50.8 mm by 286 mm drying shrinkage prisms. Capped cylinders were cured in an environmental chamber maintained at 23 °C ± 1 °C (>99 % RH), while the drying prisms were cured in the same chamber, but double bagged in plastic. Following demolding after 1 d, cylinders

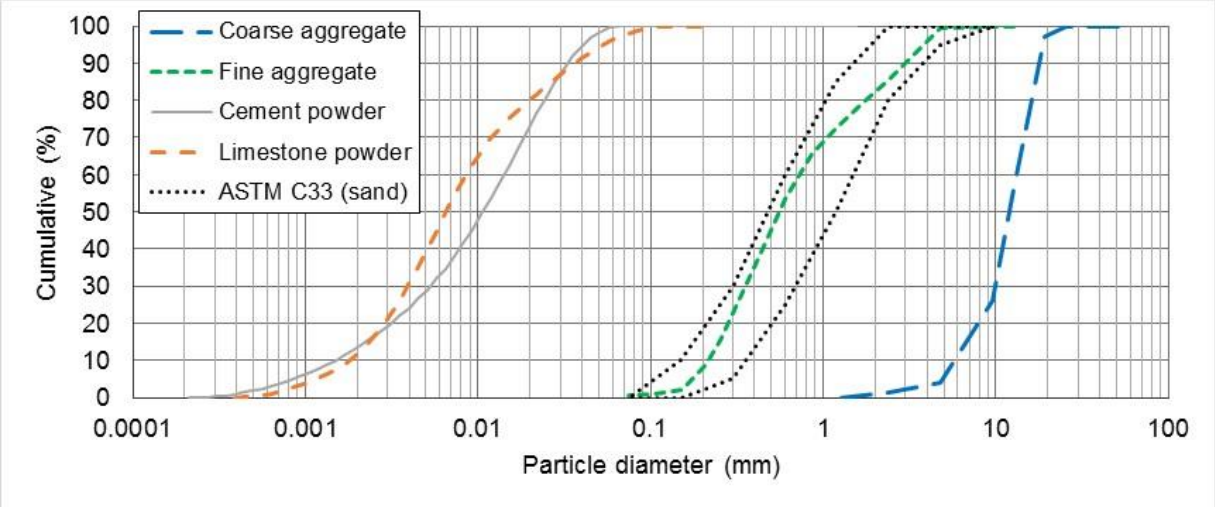

Figure 3. Cumulative particle size distributions for limestone powder, cement, sand, and coarse aggregate used in the three concrete mixtures.

Table 2. Concrete mixture proportions (kg/m^3 or L/m^3 for HRWRA)

	OPC	**6.7 µm limestone - 1**	**6.7 µm limestone - 2**
Cement	343	254.9	248.1
Limestone powder	---	127.3	178.2
Water	171.45	152.9	136.5
Fine aggregate	822	822	822
Coarse aggregate	1082	1082	1082
HRWRA C (L/m^3)	1.08	2.5	2.5
w/c	0.50	0.60	0.55
w/s	0.50	0.40	0.32
w/(c+k·LP) *k=0.25*[A]	0.50	0.533	0.466
Cement reduction	---	25.7 %	27.7 %
Cement paste volume reduction	---	16.5 %	23.2 %

[A]*k* indicates a cementing efficiency factor for the limestone, taken to be 0.25 in this study (e.g., one unit of limestone powder is assumed to be equivalent to or able to replace 0.25 units of cement).

were stored in water saturated with lime (calcium hydroxide) at 23 °C ± 1 °C until their age of testing, while the drying prisms were immersed for 2 d in the limewater and then exposed to drying in an environmental chamber maintained at 23 °C ± 2 °C and 50 % ± 2 % RH. Cylinders were broken in triplicate at the ages of 1 d, 3 d, 7 d, 14 d, and 28 d. At each of these testing ages, prior to the compression testing, the cylinders to be broken, along with any remaining cylinders, were characterized by measurements of their mass, surface electrical resistance (one device), uniaxial (bulk) electrical resistance (two separate devices, one employing a square wave with a frequency of 40 Hz and the other a sine wave with a frequency of 10 kHz), and surface ultrasonic pulse velocity (UPV). Cylinder mass measurements under saturated curing were subsequently used to estimate the chemical shrinkage occurring within the paste portion of each concrete mixture. The remaining two of the freshly cast cylinders were utilized in making continuous measurements of

electrical resistance using two different commercial devices (one modular with remote data acquisition via Bluetooth, but at a single fixed frequency of 10 kHz, the other with frequency varying from 10 Hz to 10 kHz). Finally, pore solutions were expressed from small cylindrical specimens of the hardened (sieved) mortar at various ages and their conductivity determined using one of the electrical resistance devices; for select specimens, the composition of their pore solution was also analyzed using inductively coupled plasma atomic emission spectroscopy (ICP-AES).

Results

Paste Studies

PSDs and Limestone Blends

The first question addressed in the paste portion of the current study was which combination of available limestones to blend with the cement. Both the cost and the performance of the limestone depend on its fineness. The cost of the limestone powder is highly variable, with the additional grinding (energy) required to produce the finer powders resulting in increased consumer prices. For example, the 1.6 µm limestone might cost 50 % more than the comparable 16 µm powder. However, the increased surface area provided by the finer powders provides additional nucleation sites for cement hydration products, reducing setting times, increasing early-age strengths, and reducing transport coefficients [7,10,16,17]. Improving the overall packing efficiency of the cement/limestone powder mixture could also result in a reduced water demand that would further contribute to strength increases.

Based on the PSDs in Figure 2, it was envisioned to broaden the initial cement PSD on both its fine and coarse ends by adding a blend of two different limestone powders, with the goal of increasing the maximum packing fraction of the powder component of the paste. According to Brouwers [18], for a continuous PSD, the maximum packing fraction is obtained when the cumulative PSD falls on a straight line when plotted using a logarithmic x-axis. As shown in Figure 4, the original cement appears to be far from achieving this optimal (packing) distribution, when considering 0.75 µm and 70 µm as the lower and upper endpoints for the target continuous PSD. Indeed, centrifuge measurements indicated a packing fraction of only 52.6 % for this cement powder, when initially prepared as a *w/c*=0.4 paste.

Four different blends of limestone(s) and cement were considered in the first series of pastes, with a *w/c*=0.4 ordinary cement paste considered as a reference. For these mixtures, a 50:50 mixture by mass of cement and limestone was arbitrarily employed, and the water-to-solids mass ratio (*w/s*) was fixed at 0.22 (with HRWRA)[2], with the exception of a binary blend of the 4 µm limestone powder and cement where the *w/s* was set at 0.3 and no HRWRA was used. Thus, this last mixture directly investigated the capability of limestone powder to enhance rheology and permit a water reduction without the use of HRWRA. For all of the ternary powder mixtures, a fixed 25:50:25 proportion of fine limestone (FLS):cement:coarse limestone (CLS) was employed. With a 50 % mass replacement of cement by limestone powder and a *w/s*=0.22, a reduction in cement content of about 36 % would be achieved. All of the *w/s*=0.22 pastes were prepared with a 7.5 mL/kg powder dosage of the polycarboxylate-based HRWRA A.

For these mixtures, as shown by the computed cumulative PSDs in Figure 5, the 2.2 µm limestone blended with the 16 µm limestone in equal proportions lies closest to the "ideal grading" line and also yielded the highest measured packing density (63.5 %), consistent with the theoretical

[2] While maintaining *w/c*=0.4 for a 50:50 mixture of limestone and cement would infer a *w/s*=0.2, here *w/s* was adjusted upward slightly to 0.22 with the anticipation that the limestone powder will react slightly and contribute to strength development [7].

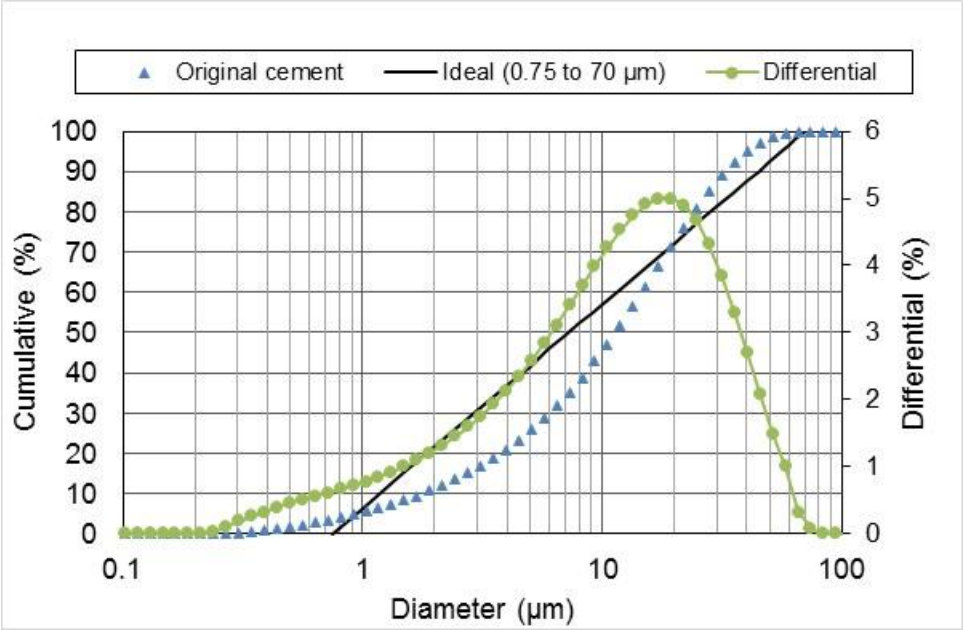

Figure 4. Cumulative PSD for original cement in comparison to "ideal" gradation [18] for optimum packing fraction. The measured result is the average of six individual measurements and the error bars (one standard deviation) would fall within the size of the shown symbols.

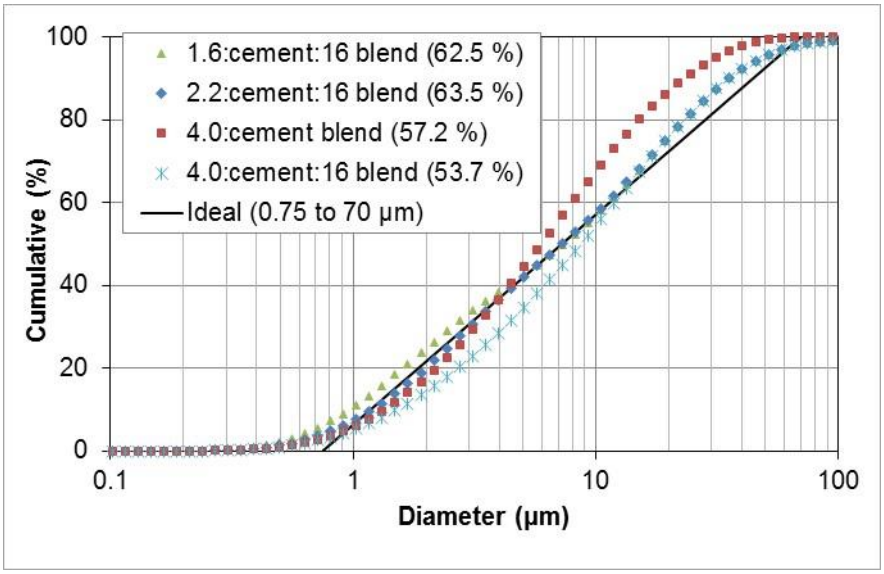

Figure 5. Computed PSDs for the cement-limestone blends. Numbers in parentheses indicates the measured packing fraction for the produced cement paste using each powder.

derivations of Brouwers [18]. Additionally, as shown in the ITC results in Figure 6 (normalized per unit volume of water in each paste mixture), the 1.6 µm and 2.2 µm limestone powders produce similar performance in terms of both the timing of the early-age calorimetry peaks and the later age cumulative heat release, the latter correlating to strength development [19]. The 25:50:25 blend prepared with the 4 µm fine and the 16 µm coarse limestone powders was not able to offset the retardation produced by the HRWRA (Figure 6, left), resulting in reduced cumulative heat release (strength) at early ages, although by 7 d, it exhibited a similar cumulative heat release value as the

other mixtures. Given its reasonable performance as assessed by calorimetry, anticipated lower cost, and slightly higher packing fraction, the 2.2 µm limestone powder was selected for blending with the 16 µm limestone in the studies that followed next.

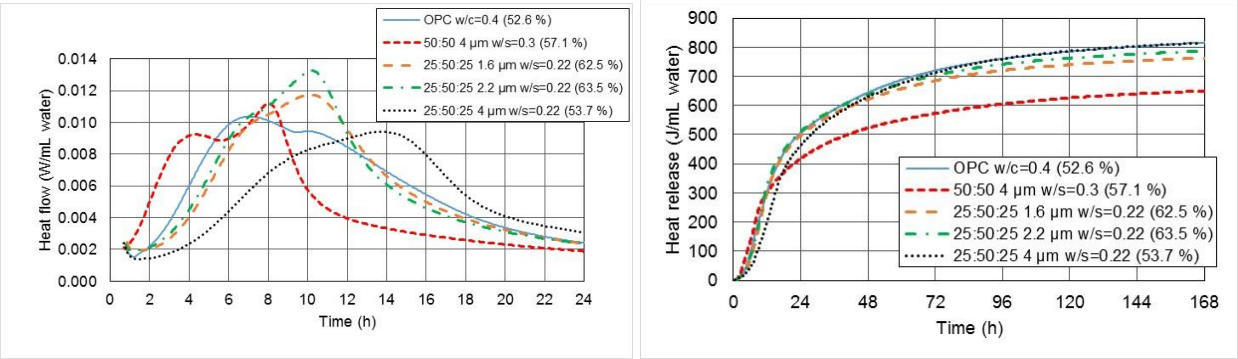

Figure 6. Heat flow (left) and cumulative heat release (right) for the cement-limestone blend pastes. The 25:50:25 mixtures all employed the 16 µm limestone as the coarse limestone component. Numbers in parentheses in legends indicate measured packing fraction for each mixture.

Binary Blend Optimization

Next, various ratios of fine (2.2 µm) to coarse (16 µm) limestone in the blended cement were considered. Here, five ratios of the two limestone powders, namely 10:90, 30:70, 50:50, 70:30, and 90:10 for the fine to coarse ratio were considered in the second paste-based study. In this phase of the study, the three powders were blended on a volumetric basis (50 % cement and 50 % limestone by volume) to account for the inherent differences in density between the cement and limestone. The *w/s* was maintained at 0.22 (cement reduction of 31 %) resulting in *w/c*=0.41. For these pastes, a second HRWRA (B) that produces less retardation was employed at a dosage of 5 mL/kg powder. As shown in Figures 7 and 8, the 50:50 mixture lies closest to the theoretical line for maximum packing and also yields the highest measured packing fraction, once again consistent with the theoretical derivations of Brouwers [18].

However, while the 50:50 mixture of the fine and coarse limestone powders is optimum from a maximum packing fraction point of view, it is the surface area of the limestone "filler" that has a much larger influence on performance, as indicated by the performance metrics presented in Figures 8-10. As the fine limestone fraction (and thus surface area) in the blend increases, the hydration is accelerated (and amplified) as indicated by the time to the first and second calorimetry peaks in Figure 8. However, this early age acceleration is accompanied by a reduction in cumulative heat release at the ages of 1 d and particularly at 7 d, perhaps due to the rapid initial precipitation of hydrates covering up cement clinker particle surfaces and reducing their subsequent reaction rates. Since cumulative heat release generally correlates well with compressive strength [19,20], the highest strength mixture would likely be the 10:90 mixture of fine:coarse limestone. Similarly, in viewing the rheology results in Figure 10, the 10:90 mixture produces the lowest stresses at all measured strains, suggesting enhanced flow at a given HRWRA dosage or alternately a lower required dosage of HRWRA to achieve a desired flow.

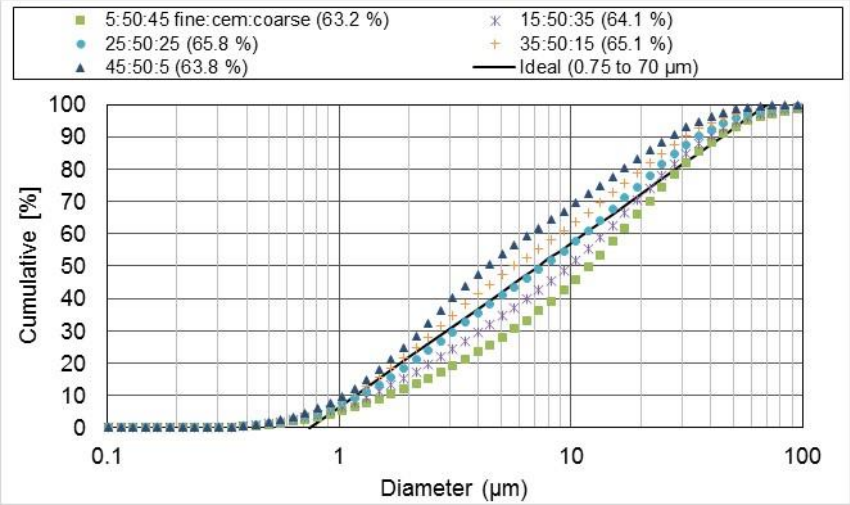

Figure 7. Computed particle size distributions for ternary blends of fine limestone:cement:coarse limestone with the indicated volumetric proportions. Numbers in parentheses in legend indicate measured packing fraction for each mixture.

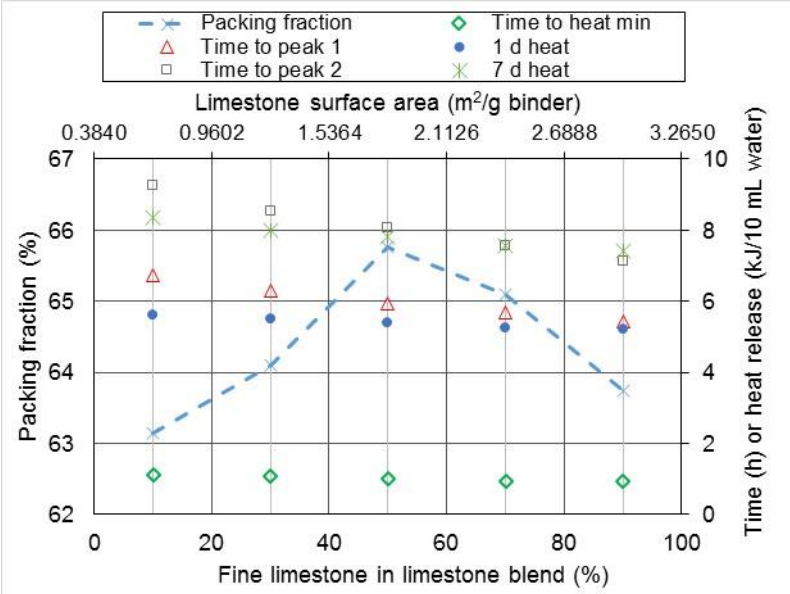

Figure 8. Measured packing fraction and ITC characteristics for pastes prepared with the ternary blends of fine limestone:cement:coarse limestone. Each mixture contains a 50:50 volumetric mixture of cement and limestone powder with the fine:coarse limestone proportions being 10:90, 30:70, 50:50, 70:30, and 90:10, as indicated by the fine limestone value on the lower x-axis.

At this point, in light of the above results and discussion, it would be fair to raise the question of whether any of the fine limestone is needed in the blended powder, given its generally negative impact on rheology and longer term cumulative heat release (and presumably strength). Indeed, in OPC concretes with 10 % limestone substituted for the cement on a volume basis investigated in a previous study [7], measured performance was similar for the 1.6 µm and 16 µm limestone powders, with the exception of setting times, where the finer limestone provided a reduced setting time relative to the coarser one. Similar results have been obtained in a recent

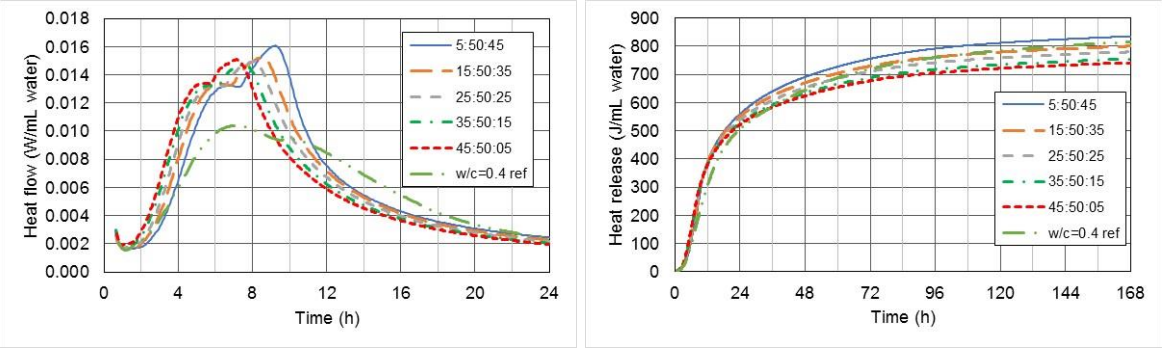

Figure 9. Heat flow (left) and cumulative heat release (right) for the cement-limestone blend pastes in phase two of the paste study. Ratios in legend indicate fine limestone:cement: coarse limestone proportions on a volume basis.

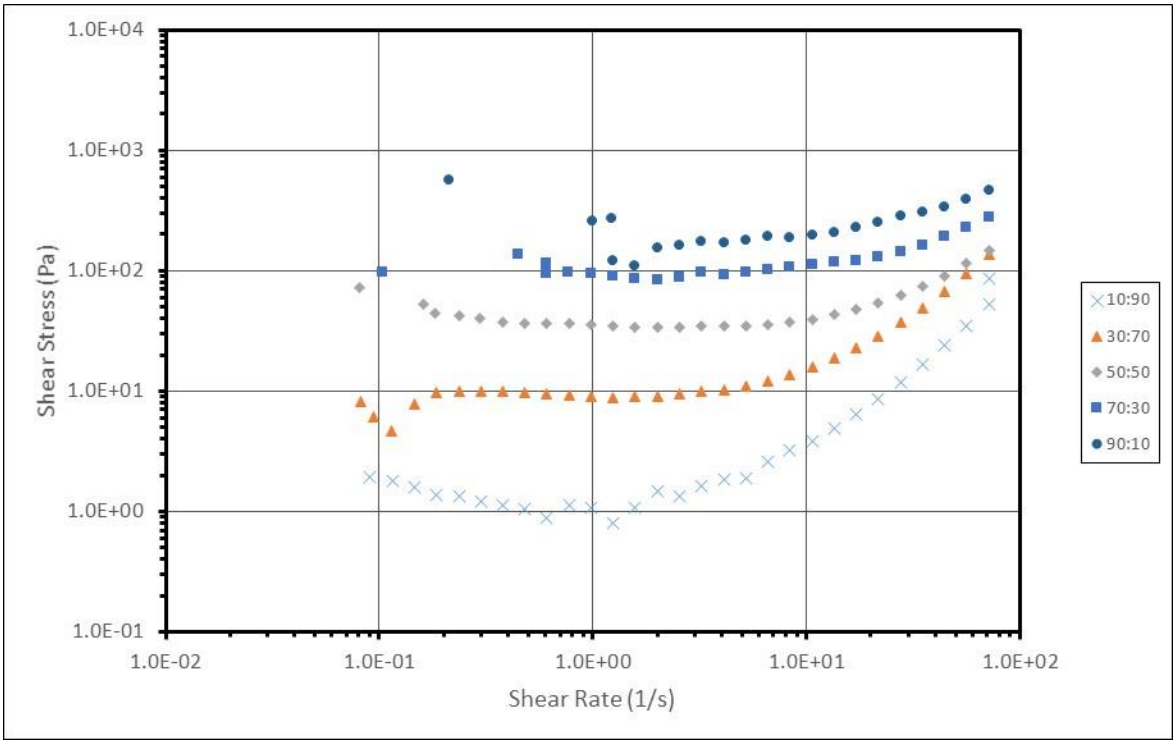

Figure 10. Shear stress vs. shear rate for parallel (serrated) plate rheological measurements for the ternary blend cement pastes. Typical relative error for viscosity is about 7 % [21].

Canadian study that compared the performance of limestone powders with median particle diameters of 3 µm and 17 µm and found basically equivalent performance [22]. Due to the requisite high dosage of HRWRA that is envisioned for the low *w/s* mixtures being developed in this study, it was decided to maintain about a 5 % proportion of the fine limestone (i.e., 10:90 fine:coarse in the 50 % limestone, 50 % cement blend) to help offset the anticipated retardation produced by the HRWRA. The initial overlap of the *w/c*=0.4 control and 5:50:45 paste heat flow curves in Figure 9 is consistent with this hypothesis. However, if some delay in the setting times, such as 1 h to 2 h, were not an issue for the field application, it is possible that acceptably performing cement/limestone powder blends could be engineered using only the 16 µm limestone powder or even the 19.2 µm one, for example, likely minimizing both costs and materials storage

requirements. This issue will be explored further in the mortar mixtures to follow where the performance of mixtures with a blend of fine and coarse limestone and with only a coarser limestone will both be contrasted against the reference *w/c*=0.4 OPC mortar.

To give an idea of the particle shapes (packing, etc.) for this ternary blend of two limestone powders with portland cement, a well-blended mixture of the 5:50:45 proportions was mounted in epoxy and imaged using a scanning electron microscope with X-ray imaging capability. Using a newly released imaging tool [23], the two-dimensional image set was processed and segmented into individual phases as shown in Figure 11. Both the fine and coarse limestone particles are clearly visible in Figure 11, with a small portion of them being identified as dolomite (magnesium carbonate) as opposed to calcite (calcium carbonate). All three powders have been produced by grinding, so that their general shapes are somewhat similar, with the limestone particles tending to be perhaps a bit more elongated and angular. The general characteristics of the particles in Figure 11 would certainly support the validity of considering their composite blend as representing a single continuous PSD of "similar" particles, for comparison to the linear-log maximum packing fraction line of Brouwers [18], as was performed in Figures 5 and 7. Thus, it is perhaps not surprising that the measured packing fractions were consistent with the theoretical predictions.

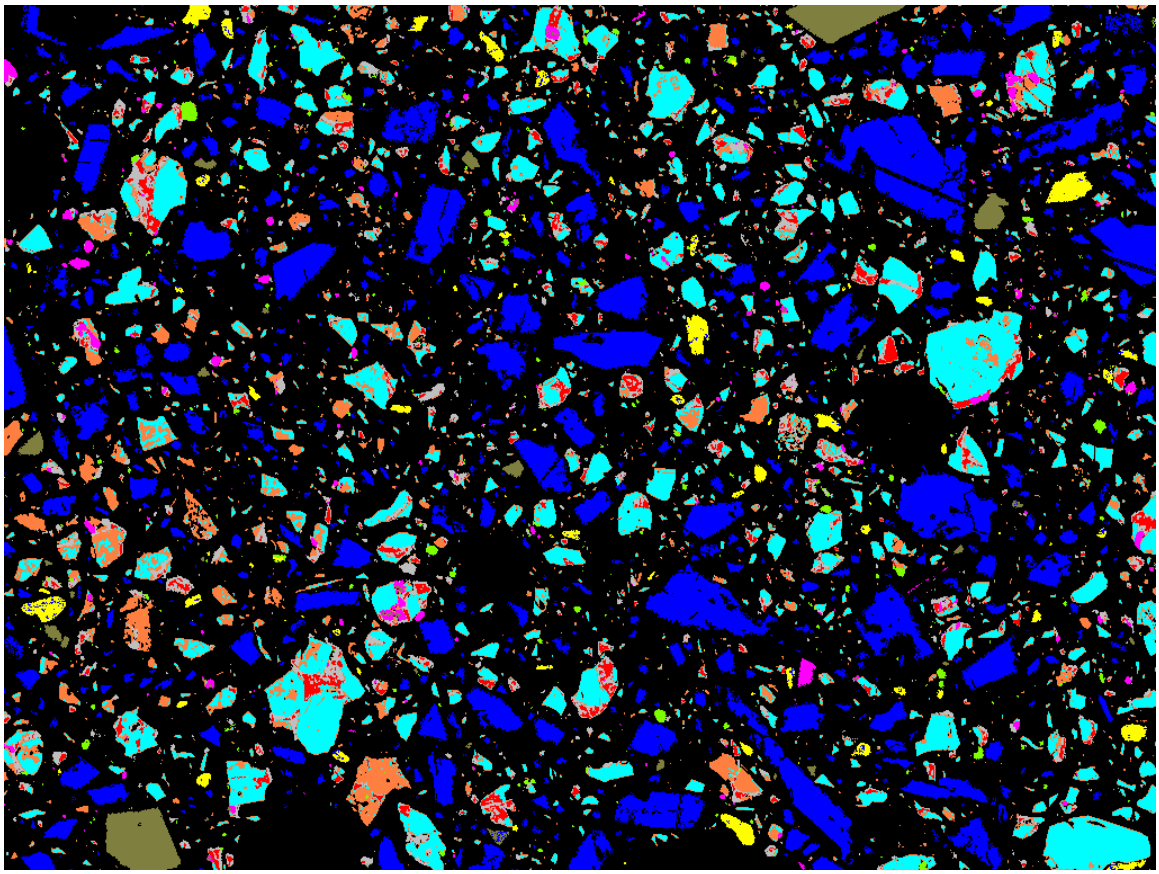

Figure 11. Color-coded SEM/X-ray image of the 5:50:45 fine limestone:cement:coarse limestone powder blend. Image shown is approximately 439 µm by 586 µm with the following color assignments: cyan – C_3S, orange – C_2S, grey – C_3A, red – C_4AF, magenta – periclase, yellow – calcium sulfate, blue – calcite, and tan – dolomite.

Mortars

For several of the mortars, the limestone content of the powder blend was reconsidered and reduced slightly to meet specific targets for *w/c* and *w/s*. Given specified target values for the mass-based *w/c* and *w/s*, the volume fraction of the cement in the powder blend can be computed as:

$$V_{cem}^{f} = \frac{1}{\left\{1-\left(\frac{\rho_{cem}}{\rho_{LS}}\right)\left[1-\frac{\left(\frac{w}{c}\right)}{\left(\frac{w}{s}\right)}\right]\right\}} \quad (1)$$

where ρ_{cem} and ρ_{LS} are the densities of the cement and limestone powder, respectively. For two of the cement-limestone blend mortars, *w/c* and *w/s* were set at 0.4 and 0.25, respectively, resulting in a volumetric-based blend of 59 % cement and 41 % limestone powder via equation 1. Maintaining *w/c*=0.4 will allow nearly all of the cement to hydrate even under sealed curing conditions, while *w/s*=0.25 was viewed as the lower end of the acceptable range for producing a flowable mortar while staying within the manufacturer-recommended range of HRWRA dosage (i.e., about 5 mL/kg of powder). Such a mixture is also consistent with a previously presented analysis based on Powers' model for cements with limestone fillers [4]. A mixture with these proportions achieves a 23.5 % reduction in cement paste (both cement and water) content for the mortar. For the *w/s*=0.25 mortars, both a 10:90 blend of the 2.2 µm and 16 µm limestone powders and just the 16 µm limestone powder by itself were used for cement paste replacement for comparison to the *w/c*=0.4 100 % OPC reference mortar. To investigate possibly more economical mixtures, three additional mortars were prepared. First, a mortar with *w/s*=0.28, *w/c*=0.52 and a 50:50 volumetric ratio of limestone to cement powder was investigated, using the 10:90 mixture of the 2.2 µm and 16 µm limestones. This mixture provides a 27.5 % reduction in cement paste content and a 37.9 % reduction in cement content. Second, two mortars with *w/s*=0.30, *w/c*=0.51 and a 44.5:55.5 volumetric ratio of limestone to cement powder were investigated using either the 6.7 µm or the 19.2 µm limestone powder, providing about a 33.6 % reduction in cement content. These two mixtures, along with the two *w/s*=0.25 mortars, provide an indication of the influence of limestone powder fineness on mortar performance. The measured fresh and hardened properties of these six mortars are summarized in Table 3, while Figures 12 through 14 provide graphical representations of their isothermal and semi-adiabatic calorimetry data.

Fresh Properties

As can be seen in Table 3, the fresh mortar temperatures of the mixtures with reduced *w/s* were a few degrees higher than the *w/c*=0.4 mortar, likely due to the extra energy imparted to the materials during (their more viscous) mixing. Air contents and flows of the *w/c*=0.4 and the *w/s*=0.25 and 0.30 mortars were generally similar, with a slightly elevated air content of 4.7 % in the *w/s*=0.30 mortar prepared with the 19.2 µm limestone powder and HRWRA C. It was noted that the *w/s*=0.25 mortars prepared with the HRWRA generally did not maintain their flow well during the approximately 1 h required to cast the various specimens being evaluated in the present study, particularly for the mixture prepared with only the coarse limestone powder. This situation was somewhat improved in the *w/s*=0.30 mortars, due to both their higher water content and to the switch to different HRWRAs (C, D, and E). The *w/s*=0.28 mortar exhibited an extremely low air content and an excessive flow, and it is likely that the HRWRA was overdosed in this particular mixture, although both cube and autogenous deformation tube specimens were castable (pourable).

Table 3. Properties of mortars investigated in the present study

	***w/c*=0.4 control**	***w/s*=0.25 LS blend**	***w/s*=0.25 16 µm LS**	***w/s*=0.28 LS blend**	***w/s*=0.30 6.7 µm LS**	***w/s*=0.30 19.2 µm LS**
Temperature (°C)	22.9	25.4	26.4	25.5	25.2	24.5
Mortar density (kg/m^3)	2.26	2.33	2.32	2.35	2.29	2.23
Air content (%)	2.6	2.5	3.0	0.4	2.3	4.7
Flow/spread (%)	118.5	106	109	Overflow	96	110
Initial "set" (h)	2.6	1.2	1.3	1.6	2.3	2.2
1-d strength (MPa)	29.8 (4.2 %)[A]	43.8 (3.0 %)	39.2 (4.7 %)	32.9 (1.1 %)	29.4 (2.2 %)	26.7 (3.0 %)
7-d strength (MPa)	55.9 (4.4 %)	68.6 (1.5 %)	65.1 (6.8 %)	60.3 (4.1 %)	55.2 (1.9 %)	49.8 (3.0 %)
28-d strength (MPa)	65.3 (0.9 %)	78.9 (1.8 %)	77.5 (6.4 %)	77.5 (2.7 %)[B]	58.2 (2.9 %)	59.3 (0.3 %)[C]
91-d strength (MPa)	80.6 (3.5 %)	92.8 (4.3 %)	82.3 (4.0 %)	81.0 (3.3 %)	68.1 (4.2 %)	61.4[D]
7-d autogenous shrinkage (µstrain)	185	157	196	116	99	94
28-d autogenous shrinkage (µstrain)	286	203	246	155	160	147
28-d drying shrinkage (µstrain)	800	605	560	Not Measured	600	620
Ultimate drying shrinkage via ASTM C596 (µstrain)	945	685	640	Not measured	690	780

[A]Numbers in parentheses indicate coefficient of variation for three replicate specimens, or two specimens where noted.
[B]Tested at 56 d.
[C]Average of only two test specimens.
[D]Only one specimen tested.

While the early-age calorimetry curves are similar in Figures 12 and 14 (up to 5 h for example), the *w/s*=0.25 and *w/s*=0.28 mortars did set about an hour earlier than the *w/c*=0.4 mortar, likely due to both their reduced water content [24] and their rapidly stiffening (denser) matrix (loss of flow mentioned earlier). This earlier setting could potentially be a problem in field concrete mixtures that might have to be addressed by the addition of a retarder, for example.

Calorimetry

Figure 12 shows the heat flow results normalized both per unit mass of cement and per unit volume of water (since *w/c* is variable in the different mortars). Clearly, the addition of any of the limestone powders to the mortar is providing an amplification of both the silicate and aluminate hydration reactions [7,10,16]. It is probable that the additional surface area provided by the limestone powder(s) is also accelerating these reactions, but that effect is likely masked by the retardation produced by the substantial dosage of HRWRA required in these mixtures. This enhanced hydration should contribute to an increase in early-age compressive strength [19] in these mortars, consistent with the measured increases shown in Table 3, particularly when the finer limestone powders are employed. This effect can be seen more clearly in Figure 13 that shows the cumulative heat release normalized per unit volume of initial (mixing) water vs. age for the six mortars; here, it can be observed that the heat release of the two *w/s*=0.25 mortars exceeds that of the *w/c*=0.4 mortars at ages beyond about 6 h, with the maximum deviation occurring at approximately 24 h. In terms of both isothermal and semi-adiabatic calorimetry, for the *w/s*=0.25 mixtures, the differences between the limestone powder blend and the coarser limestone powder only are minimal, as are the differences for the two *w/s*=0.3 mortars prepared with different size limestone powders.

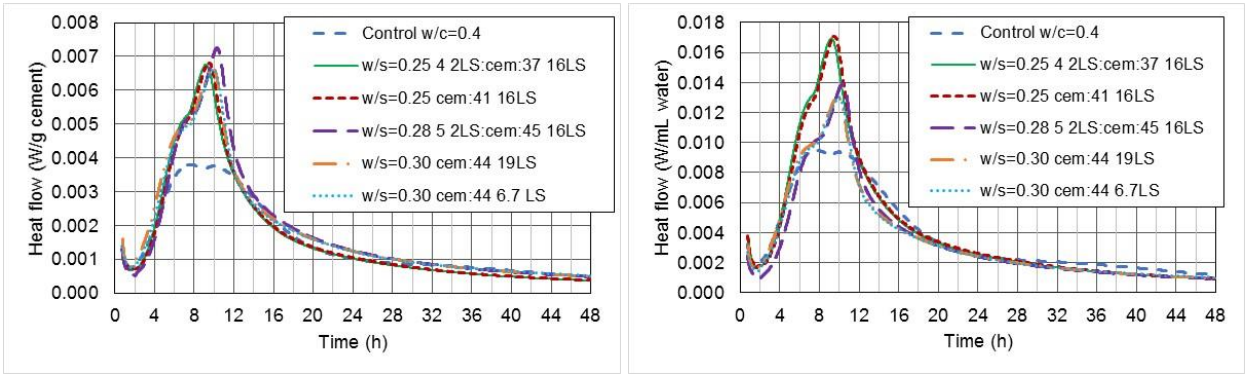

Figure 12. Heat flow normalized per mass of cement (left) and per volume of initial water in the specimen (right) vs. time for the six mortars.

Interestingly, the semi-adiabatic temperature rise curves shown in Figure 14 are fairly similar for the six mortars, particularly for the reference and *w/s*=0.25 mortars. While the *w/c*=0.4 reference mortar contains 23.6 % more reactive cement per unit volume of material relative to the *w/s*=0.25 mixtures, it also has an increased heat capacity due to the 23.6 % increase in water, with its corresponding relatively high heat capacity of 4.18 J/(g·K). These two factors, along with any amplification of the hydration reactions provided by the limestone powder(s), balance each other out, so that the semi-adiabatic temperature response for the ≈375 g mortar specimens investigated in the present study are all quite similar. The peak temperatures achieved for the *w/s*=0.28 and

w/s=0.30 mixtures are about two to four degrees less than that observed for the other three mortars, due to their increased water content relative to the *w/s*=0.25 mortars, for example. For these mortars, there is also some indication of enhanced reactivity at the later ages of 36 h to 72 h where several shallow fairly broad peaks in temperature are observed in Figure 14.

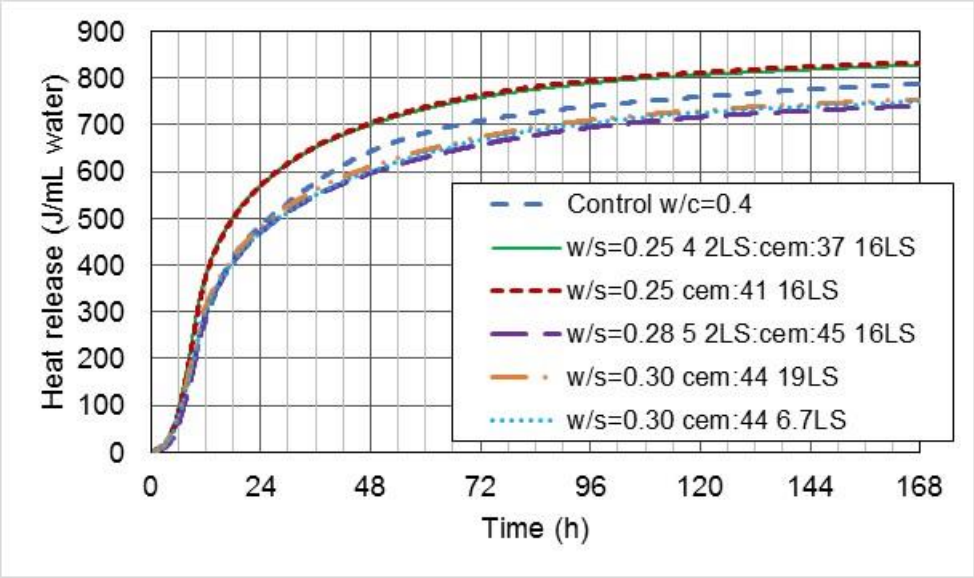

Figure 13. Cumulative heat release vs. time for the six mortar specimens.

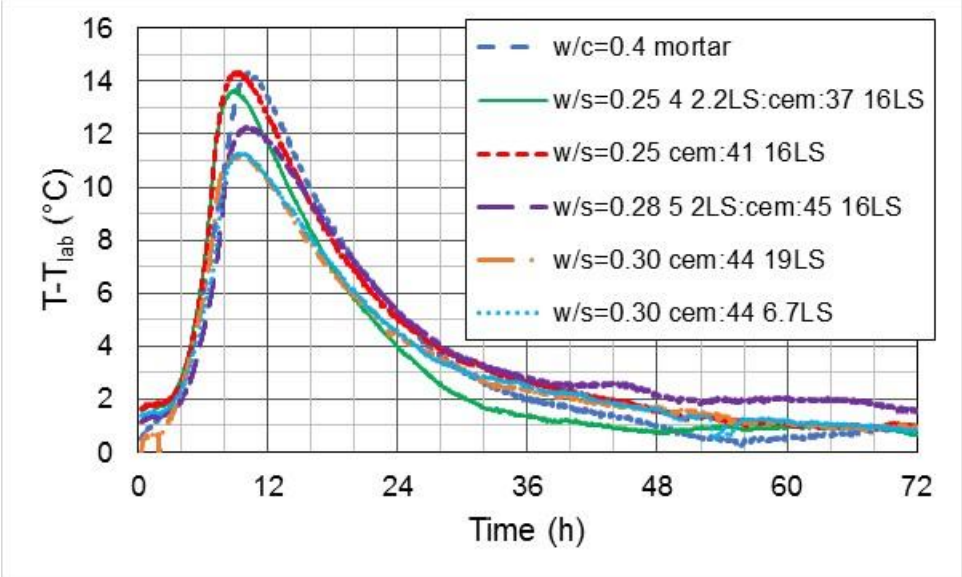

Figure 14. Semi-adiabatic temperature vs. time for mortars investigated in the present study.

Compressive Strength

The compressive strength results in Table 3 indicate that the *w/s*=0.25 and *w/*s=0.28 mortars have higher strengths at all ages than the *w/c*=0.4 control. Generally, concrete strength is related to *w/c* [3], so it might be expected that the three mortars with equivalent *w/c* would exhibit equivalent strengths (at equivalent degrees of hydration, for example). While a portion of the

measured strength increases is surely due to the amplification of the hydration reactions as indicated in Figures 12 and 13, plotting strength vs. heat release (Figure 15) indicates an additional contribution to strength, particularly in the two mortars prepared with the 10:90 blend of fine and coarse limestone powders. This additional strength may be due to the enhanced particle packing provided by the blended limestone powder, as well as the ability of its surfaces to serve as nucleation and growth sites for hydration products. In this way, the limestone particles become an integrated component of the three-dimensional (percolated) network of particles and hydration products that provides setting and strength to the developing microstructure [7]. Specifically, the blend of fine and coarse limestone powders outperforms the use of the coarse limestone powder by itself in the *w/s*=0.25 mortars, producing a 5 % to 10 % increase in measured compressive strengths at ages of 1 d, 7 d, and 91 d. All of the measured variations for compressive strength listed in Table 3 are within the range of variations permitted by ASTM C-109 (8.7 % for three cubes and 7.6 % for two cubes) [9].

In terms of matching the compressive strength development of the *w/c*=0.4 reference mortar, the initial *w/s*=0.25 mortars provided an excess, suggesting that further cement reductions could be implemented. Specifically, the current limestone replacement level in the *w/s*=0.25 mortars produces strength increases (relative to the reference *w/c*=0.4 mortar) on the order of 32 % to 47 % at 1 d, 16 % to 23 % at 7 d, 19 % to 21 % at 28 d, and 2 % to 15 % at 91 d. To maintain the conditions specified by equation (1) while maintaining *w/s* at 0.25, the required reduction in cement would produce a concurrent increase in the *w/c* ratio of the limestone blended paste above its current value of 0.4, similar to the *w/c*=0.52 that was produced in the *w/s*=0.28 mortar and the *w/c*=0.51 used in the *w/s*=0.30 mortars. The *w/s*=0.28 mortar did produce strengths that were basically equivalent or slightly superior to those of the *w/c*=0.4 reference mortar at all ages, while the *w/s*=0.30 mortar with the 6.7 µm limestone powder produced similar strengths to the reference at ages of 1 d and 7 d, before falling behind at the later ages of 28 d and 91 d, ultimately producing about 85 % of the reference strength value at 91 d.

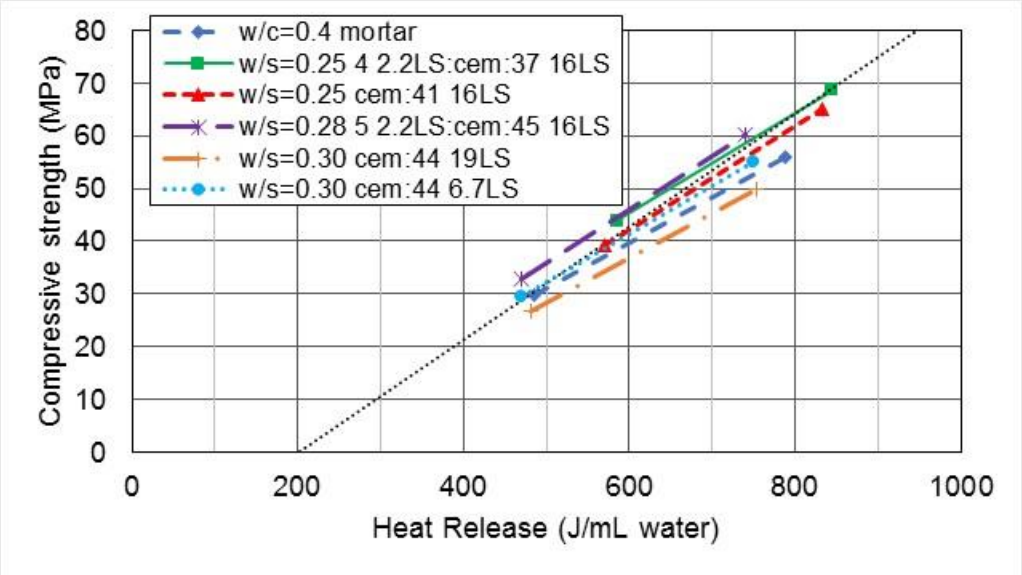

Figure 15. Compressive strength vs. cumulative heat release for the six mortars measured at 1 d and 7 d. Coefficients of variation for strength measurements are given in Table 3. Dotted line indicates a best fit relationship determined for a variety of mortars in a previous study [19].

Autogenous and Drying Shrinkage

The shrinkage results of the mortars (Table 3 and Figure 16) are particularly intriguing. The autogenous deformation results in Figure 16 indicate less shrinkage for the limestone-containing mortars, up to nearly 50 % less than that of the *w/c*=0.4 OPC reference mortar for the *w/s*=0.30 blended limestone mortars, for example. The addition of the limestone particles, reducing *w/s*, should also reduce the interparticle spacing and thus the size of the water-filled capillary pores [2]. Normally, this would produce an increase in autogenous shrinkage as the largest of these pores begin to empty [25], but in these mortars, this increase is counterbalanced by the significant decrease in paste content, as the paste (cement and water) is the major component contributing to the shrinkage of the mortar, as opposed to the effectively non-shrinking sand and limestone powder particles. It is interesting to note that the autogenous shrinkage of the *w/s*=0.25 mixture with only the coarse limestone powder during the first day is increased relative to that experienced by the mortar with the blend of fine and coarse limestones. The increased stiffness (strength) of the latter mixture due to the enhanced reactivity of the finer limestone and a more efficient particle packing may contribute to this reduction in strain, assuming the internal stresses in the two mortars to be approximately equivalent.

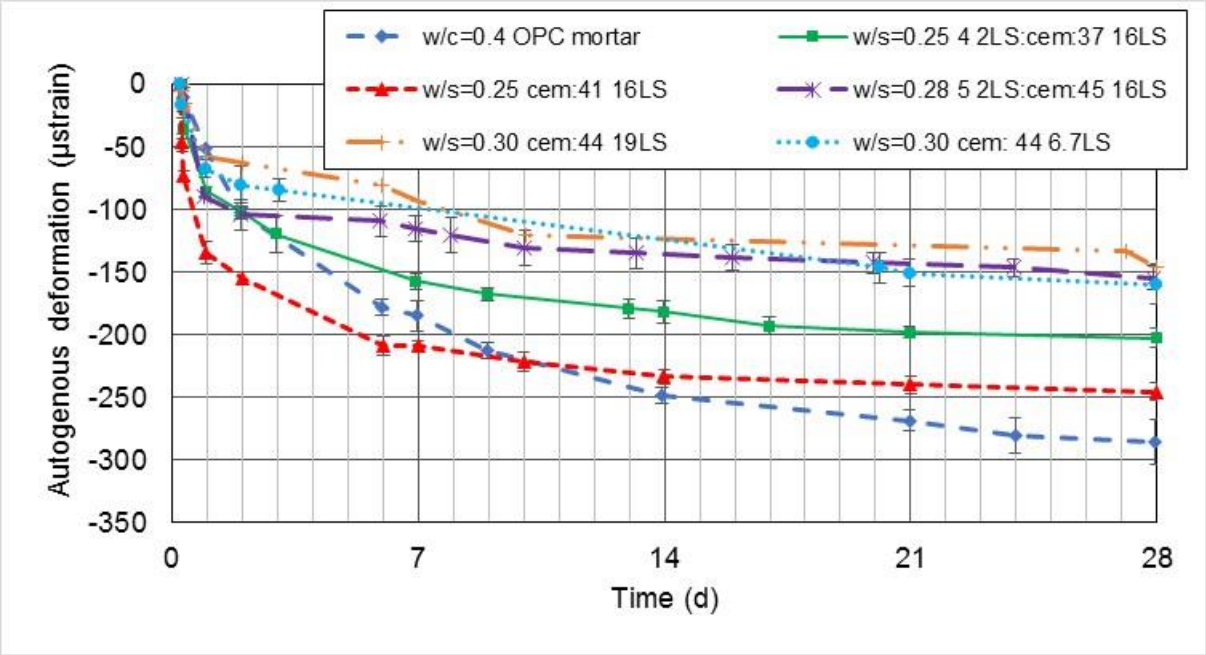

Figure 16. Autogenous deformation measured for the six mortars during the course of 28 d. Error bars indicate standard deviation for either two or three replicate specimens.

Another potential contribution to the reduced autogenous shrinkage in the mortars containing limestone powder replacements is its stabilization of ettringite, due to the formation of carboaluminate phases as opposed to sulfoaluminates [26,27]. At early ages, ettringite forms as needles that can contribute to an autogenous expansion that is commonly overwhelmed by the greater ongoing autogenous shrinkage (due to chemical shrinkage). When sulfate is depleted from the system, these ettringite needles become unstable and dissolve to form sulfoaluminate phases of a different morphology, removing their restraint and likely introducing additional autogenous shrinkage. Thus, when the ettringite is stabilized by the presence of the limestone powder, this

contribution to autogenous shrinkage will be removed. This hypothesis has been recently verified in two repair mortars that generate substantial ettringite by replacing 5 % of the repair mortar with the 16 µm limestone powder and observing a reduction (of greater than 5 %) in their measured autogenous shrinkage [28]. This stabilization of ettringite could also contribute to the increased strengths observed in the cement-limestone blended mortars, as the dissolution of ettringite needles to form monosulfoaluminate phases would also be expected to weaken (at least temporarily) the three-dimensional microstructure.

This improvement in shrinkage performance due to the replacement of cement paste with limestone powder also carries over to the drying shrinkage values given in Table 3. Perhaps not surprisingly, the observed reductions in drying shrinkage correspond closely to the 23.6 % reduction in cement paste content in the *w/s*=0.25 cement/limestone blended mortars (constant *w/c*=0.4), as once again, it is basically only the paste component that is subject to drying shrinkage. The reduced paste (water) content thus leads to a proportional reduction in drying shrinkage (and mass loss). Similarly, the shrinkage reduction is slightly less dramatic in the *w/s*=0.30 mortars due to their relatively higher water content (*w/c*).

These reductions in shrinkage could produce concretes that are more resistant to early-age cracking, a problem that has plagued bridge decks and other concrete structures for many years [29]. The HVLP mixtures are particularly intriguing in that they can provide increases in compressive strengths along with concurrent reductions in shrinkage, as most mixture modifications that will increase strength (reduction in *w/c* or *w/s*, finer cement, etc.) generally also produce increases in shrinkage, particularly autogenous shrinkage [14,24,30,31]. In the HVLP mixtures, however, the limestone powder allows for a substantial reduction in paste content and stabilization of the ettringite (reducing shrinkage), while accelerating/amplifying cement hydration and contributing to the developing solid framework that is responsible for setting and (increased) strength. These benefits of HVLP mixtures were investigated further in a set of concrete mixtures as discussed in the section that follows.

Concretes

The composite cumulative particle size distributions for the dry ingredients (limestone powder, cement, sand, and coarse aggregate) for each of the three concrete mixtures are provided in Figure 17. While the overall PSD does not follow a linear trend (on the logarithmic x-scale), arbitrarily setting a cutoff of 200 μm (0.2 mm) as the delineation between powder and aggregates produces two data subsets that are each roughly linear. In this regard, the powder components of the limestone powder concretes lie closer to the theoretical line [18] than that of the OPC mixture.

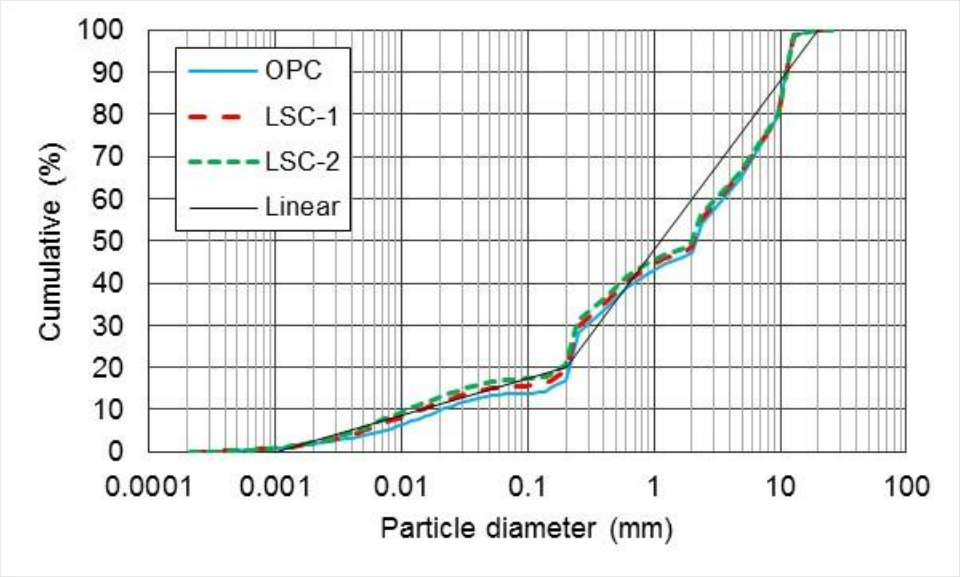

Figure 17. Cumulative particle size distributions for the three concrete mixtures.

Fresh Properties

The fresh concrete properties for the three concrete mixtures are summarized in Table 4. Given the significantly higher slump of the first mixture prepared with the limestone powder, the second mixture was prepared with less water and more limestone powder (to increase strength and decrease slump, as opposed to with less HRWRA that likely would have only reduced slump) and did achieve the desired effect of a slump more similar to that of the OPC control. All three of the mixtures have a hardened air content (AC) that is quite representative of typical non-air entrained concrete prepared in a laboratory setting. The lower fresh air content of the first limestone concrete mixture is unexplained at this time, but it should be noted that the sample for the unit weight measurement (air content determination) was obtained directly from the concrete following the slump measurement without remixing. For the second mixture with limestone, unit weights were obtained on both slump-tested and fresh from the mixer concrete, with both values being provided in Table 4. For this third mixture, the slump-tested concrete exhibited a fresh air content of 1.4 % vs. 1.8 % for the concrete freshly discharged from the mixer.

Table 4. Fresh concrete properties (see Materials and Methods for typical uncertainties)

	OPC	6.7 µm limestone – 1	6.7 µm limestone - 2
Temperature (°C)	26.8	25.3	26.1
Slump (cm)	14.6	24.1	17.1
Unit weight (kg/m^3)	2390	2450	s=2480 , f=2470 [A]
Fresh air content (%)	3.1	1.5	s=1.4, f= 1.8
Hardened AC (%)	2.9	3.5	2.5
C403 initial set (h)	4.2	3.9	2.9
C403 final set (h)	5.6	5.5	4.3

[A]s=slump test concrete; f= freshly discharged concrete

Setting Times

The setting time measurements performed on the sieved mortar via Vicat needle (ASTM C191) and penetrometer (ASTM C403) are provided in Figure 18 and summarized in Table 4. The ASTM C191 test method is strictly only applicable to cement paste, but has been applied here to mortar without any modifications. Since they are based on different critical resistance levels obtained under different loading conditions, it is not surprising that the initial setting times via the Vicat needle precede those determined using the penetrometer by about 1 h (3 h vs. 4 h). Although their mixture proportions are significantly different, the OPC control and the first mixture prepared with the limestone powder exhibit quite similar setting behavior. It appears that any retardation produced by the higher dosage of the HRWRA used in the limestone mixture is offset by its reduced water content (more solids per unit volume) and any acceleration provided by the fine limestone powder surfaces, such that the setting behaviors of the two mixtures are nearly identical. This would be beneficial to a contractor in the field, as they would not need to adjust their schedule of operations when switching from the OPC to the limestone powder concrete mixture. Because of its further reduced water content and some acceleration and amplification of its early-age hydration, the second mixture prepared with limestone powder exhibited about a 1.3 h reduction in setting times relative to the OPC and first limestone mixture. If this were to present a problem for field use, a mild dosage of a chemical retarder might be required to extend the setting times back towards those measured for the OPC and first limestone concretes. On the other hand, during the winter construction season, such a mixture might be ideal in its current form.

Early-Age Properties

Electrical resistance and ITC heat flow measurements obtained for the three mixtures during the first 24 h of curing are compared in Figures 19 and 20, respectively. The ITC was conducted at a temperature of 23.00 °C ± 0.01 °C, while the temperature (measured) of the concrete in the electrical resistance cylinders ranged between 24 °C and 28 °C (in a controlled environment maintained at 24 °C ± 0.5 °C) for all mixtures. In comparing the results from the modular and tabletop electrical resistance units in Figure 19, excellent agreement is observed for the first limestone mixture, while a systematic difference (of about 15 %) is observed for the other two mixtures, perhaps due to some consolidation variations with the stiffer (lower slump) concretes.

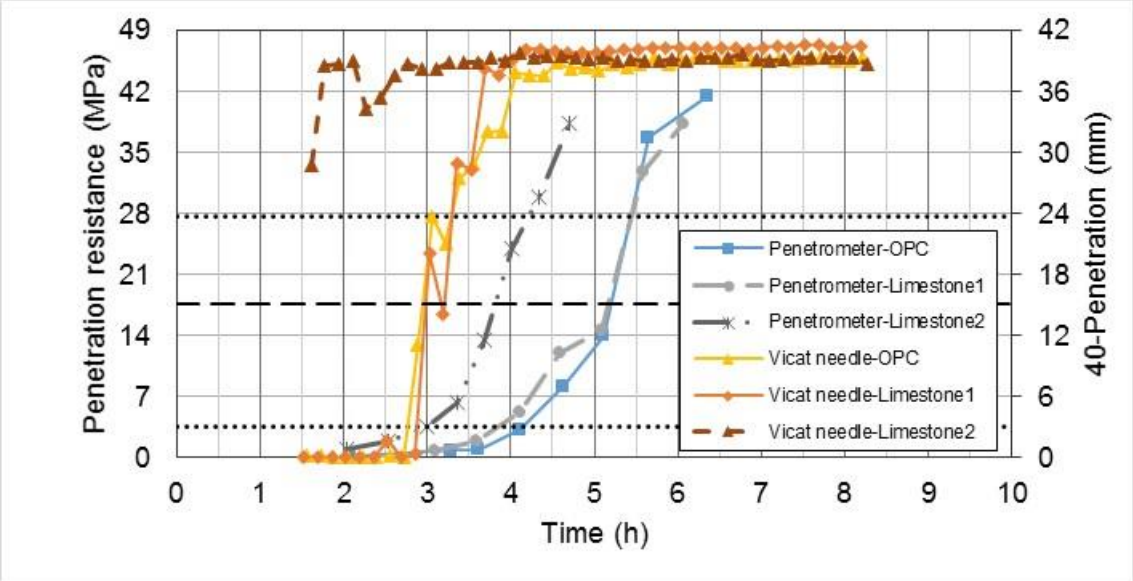

Figure 18. Measured setting times for mortars sieved from the three concrete mixtures, via both Vicat needle and penetrometer. Lower and upper dotted lines indicate resistances corresponding to initial and final setting times, respectively, via the penetrometer (ASTM C403), while the dashed line indicates initial setting criteria for the Vicat needle (ASTM C191).

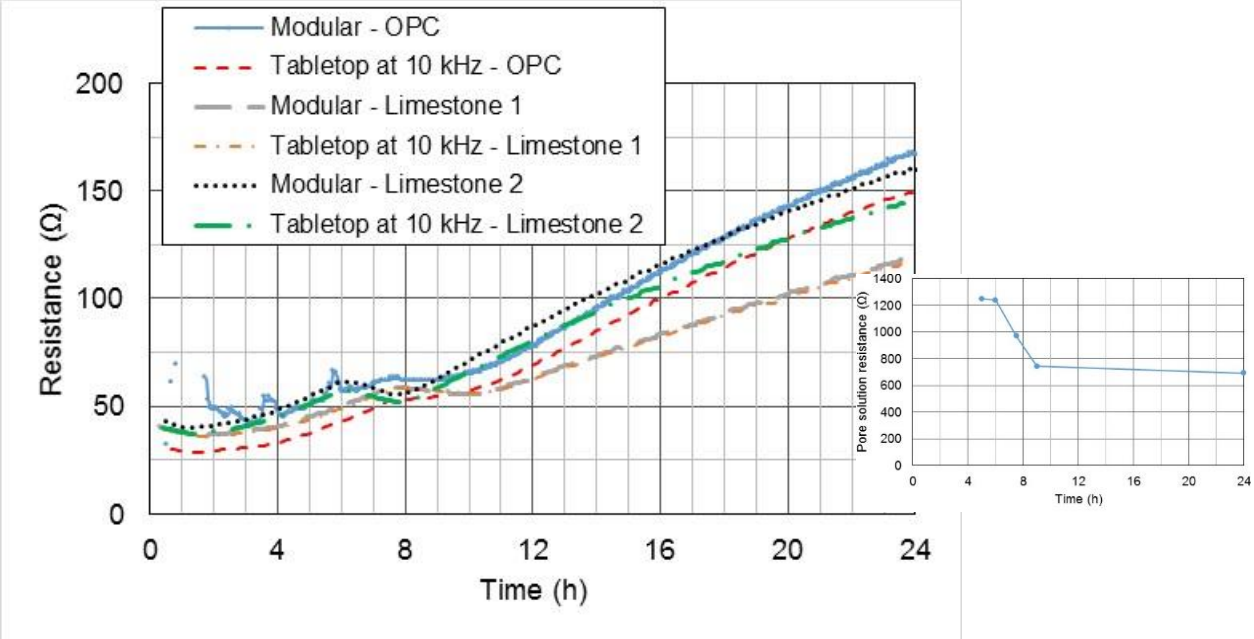

Figure 19. Measured electrical resistance (fresh concrete) for the three concrete mixtures. Inset plot shows measured (expressed) pore solution resistance for the limestone 2 concrete mixture.

Initially, for the tabletop unit measurements, the electrical resistance of the limestone mixtures (*w/c*=0.6 or 0.55) is slightly higher than that measured for the OPC mixture (*w/c*=0.50), likely due to the cement dilution producing a less concentrated pore solution (with a lower ionic conductivity). Following an increase in resistivity with time that begins between 1 h and 2 h, starting just before 8 h for the OPC and first limestone mixture and just before 6 h for the second

limestone mixture, the OPC mixture experiences a plateau, while the limestone mixtures actually decrease somewhat over the course of 2 h or so, before all mixtures continue their gradual increase. This is likely related to both microstructural and pore solution changes induced by the renewed hydration of the clinker phases as sulfate is depleted in these mixtures. One example of a microstructural alteration that could decrease resistivity would be the dissolution of ettringite (needles), which subsequently reprecipitates as other sulfoaluminate and carboaluminate phases. As sulfates are depleted from the pore solution, the hydroxide ion concentration (along with the solution pH) increases dramatically [32]; this would likely decrease the resistivity (increase the conductivity) of the pore solution and concurrently decrease the measured resistance of the concrete specimen. In support of this, measured resistances for small volumes (1 mL or so) of pore solutions expressed (squeezed) from hardened mortar specimens of the second limestone concrete mixture at early ages are shown in the inset of Figure 19. A dramatic decrease in resistance is observed during the same time window when the measured concrete specimen resistance is decreasing (e.g., 6 h to 9 h time window). Further compositional analysis was conducted on the expressed pore solutions for the limestone 2 concrete mixture and the results are provided in Figure 21. The depletion of sulfate, along with a concurrent decrease in calcium and increases in aluminum and silica are all consistent with the depletion of calcium sulfate (gypsum) and a renewed reactivity of the cement clinker (aluminate and silicate) phases during this time period.

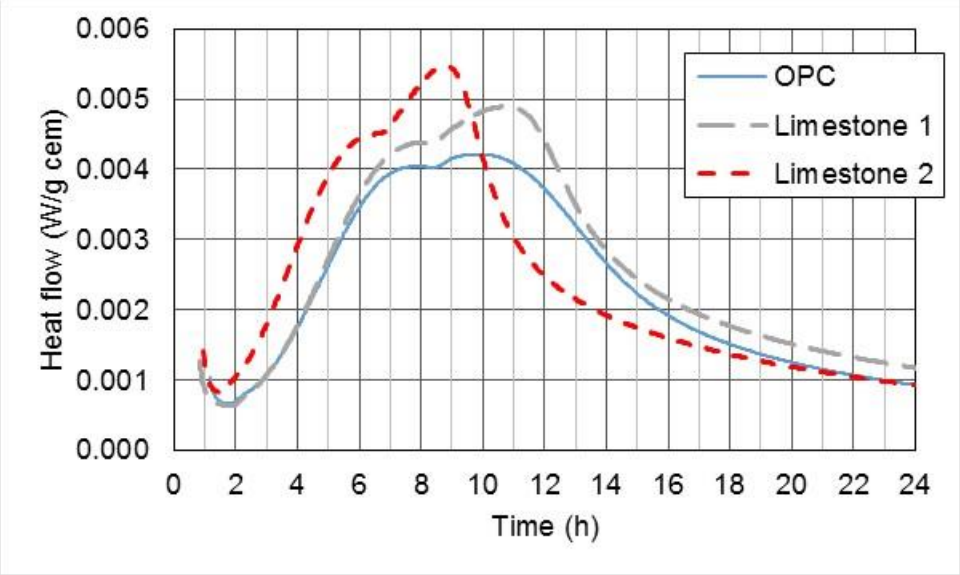

Figure 20. Measured ITC heat flow (sieved mortar) for the three concrete mixtures.

The additional carbonate ions present in the system with limestone intensify this effect, as evidenced also in the ITC curves in Figure 20, where a substantially greater heat flow is observed during this time period in the systems with the additional limestone powder than that found in the OPC mixture. This is especially noticeable for the limestone 2 concrete mixture with its higher limestone powder (surface area) to cement ratio (see Table 2). The isothermal calorimetry curves also support the setting time measurements in that the initial rise following the induction period for the various mixtures all occur within the same time frame (1.5 h to 4 h), with that of the limestone 2 concrete mixture occurring slightly earlier than those of the other two mixtures. Any retardation caused by the additional HRWRA used in the limestone mixtures has been offset by the acceleration provided by the nucleation and growth sites offered by the fine limestone particle

surfaces [7,10]. The limestone 2 concrete mixture provides 43 % more limestone surface area per unit cement than its limestone 1 counterpart, obviously leading to additional acceleration and amplification of the early-age hydration reactions (Figure 20).

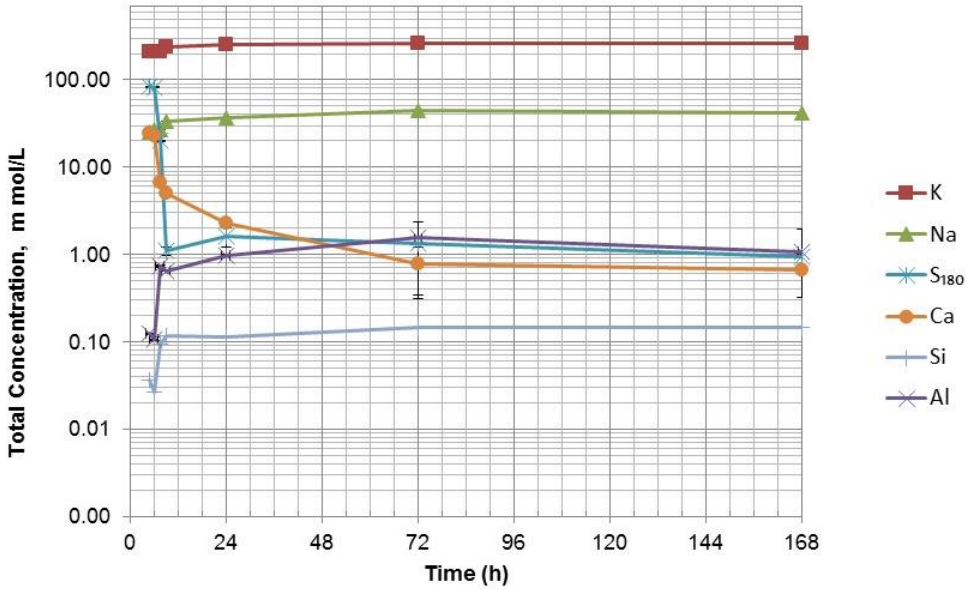

Figure 21. Chemical (ICP) analysis for pore solutions expressed from the limestone 2 concrete mixture. Error bars indicate one standard deviation for three replicate measurements at each time.

The cumulative heat release curves normalized on either a unit mass of cement or a unit volume (mass) of water basis are provided in Figure 22. The enhanced reactivity of the cement produced by the limestone additions is indicated by the cumulative heat of these mixtures exceeding that of the OPC mixture at ages beyond about 12 h for the data normalized per unit mass of cement (see also Figure 20). Conversely, when the data are normalized by unit volume of (mixing) water in each concrete mixture, the cumulative heat produced in the two mixtures with limestone falls below that of the OPC control, once again after about 12 h. As will be shown subsequently, the cumulative heat normalized per unit volume of water is a good indicator of strength development in these different concrete mixtures [16,19,20].

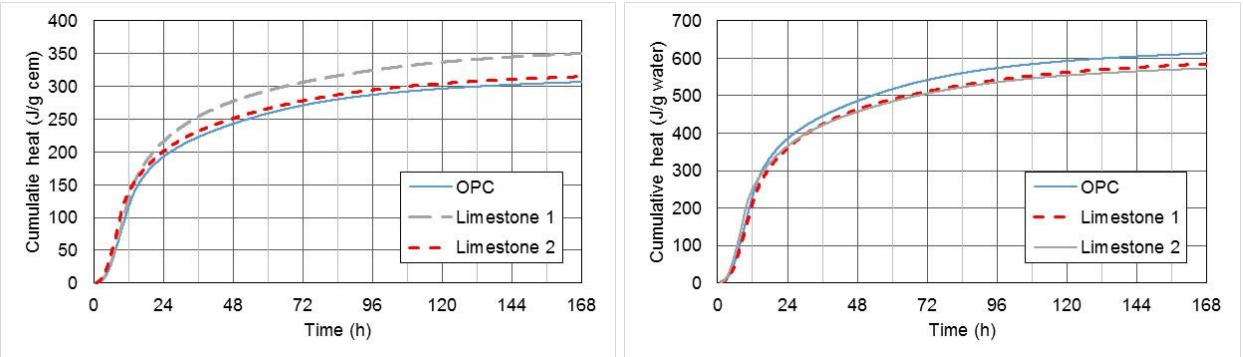

Figure 22. Cumulative heat release from ITC measurements on mortars vs. time for the concrete mixtures, normalized by either mass of cement (left) or mass of water (right).

The mass gains of the cylinders during their curing in lime water were used to estimate the ongoing chemical shrinkage in their cementitious binder as an alternate indication of reactivity. The obtained results are provided in Figure 23, where the initial acceleration provided by the limestone powder surfaces is clearly indicated. While the first limestone mixture remains above the OPC curve at all ages as it capillary porosity likely remains percolated (see Table 6 below), the limestone 2 mixture approaches the OPC values and falls below it at later ages, as the capillary porosity in this mixture likely becomes depercolated, limiting the rate at which lime water can be imbibed into the cylinders from the curing tank and concurrently reducing their hydration rate.

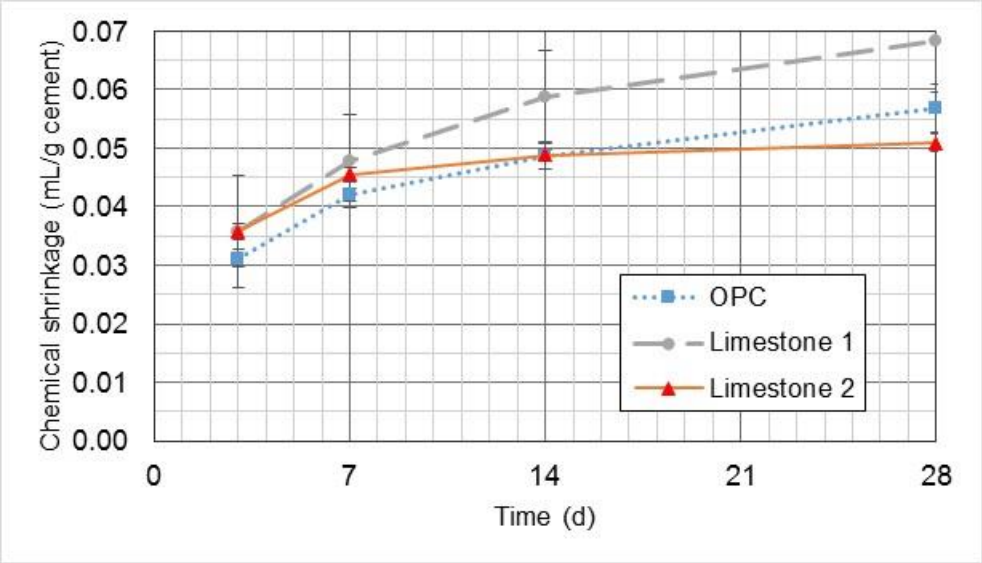

Figure 23. Estimated chemical shrinkage vs. time for the three concrete mixtures. Error bars indicate standard deviation for six replicate specimens.

Compressive Strength and Drying Shrinkage

The measured compressive strengths and drying shrinkages for the three concrete mixtures are provided in Table 5. While the first limestone mixture produced compressive strengths that were between 10 % (1 d) and 2 % (3 d) lower than those of the OPC concrete reference, the second mixture with a further reduced water content significantly surpassed (by 13 % to 20 %) the strength developed in the OPC mixture at all ages, even though it contains 27.7 % less cement. The measured drying shrinkages are plotted against the measured mass losses for each of the three concrete mixtures in Figure 24. While a linear relationship with a high correlation coefficient is obtained for each mixture, the drying shrinkage to mass loss relationship is not universal across these three mixtures, as the mixtures with limestone powder have a higher mass loss due to their higher *w/c* ratio (more evaporable water per unit cement) but exhibit less shrinkage for a given mass loss (consistent with their lower paste content in Table 2).

Relating Strength to Measurements of UPV, Heat Release, and Electrical Resistance

A comparison of the compressive strength measurements with the measured ultrasonic pulse velocity (UPV) using a handheld surface unit is provided in Figure 25. For any given mixture, the data for the various testing ages exhibits a highly linear relationship ($r^2 > 0.99$), but the slope

Table 5. Measured compressive strengths and drying shrinkage for the three concrete mixtures

	OPC	**6.7 µm limestone - 1**	**6.7 µm limestone – 2**
1-d strength (MPa)	17.9 (1.5 %)[A]	16.1 (1.3 %)	21.4 (2.7 %)
3-d strength (MPa)	29.0 (1.0 %)	28.3 (2.3 %)	34.2 (1.1 %)
7-d strength (MPa)	34.2 (1.7 %)	32.9 (2.7 %)	38.9 (1.4 %)
14-d strength (MPa)	36.7 (1.6 %)	35.8 (3.3 %)	43.5 (0.2 %)
28-d strength (MPa)	40.5 (2.8 %)	38.2 (1.6 %)	47.4 (1.7 %)
28-d drying shrinkage (µstrain)	380 (3.5 %)	400 (3.0 %)	290 (12 %)
Ultimate drying shrinkage (µstrain)	470	480	390

[A]Number in parentheses indicates coefficient of variation for three replicate specimens for strength and four replicate specimens for drying shrinkage, except for strength measurements on the limestone 2 concrete mixture at 1 d and 3 d where five specimens were tested and 7 d where four specimens were tested and for drying shrinkage on the limestone 2 concrete mixture where only two specimens were evaluated.

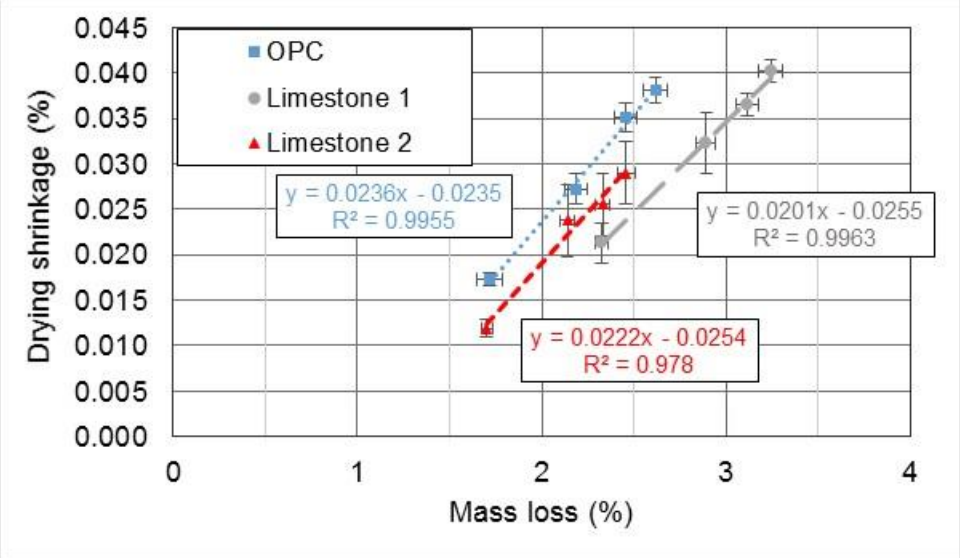

Figure 24. Measured drying shrinkage vs. mass loss for the three concrete mixtures. Error bars indicate one standard deviation for measurements of four replicate specimens (only two for the limestone 2 concrete mixture).

and intercept are variable depending on the specific mixture proportions, as has generally been observed previously when comparing UPV to compressive strength data [33]. For these concretes all prepared using the same aggregates and same volume fractions of fine and coarse aggregates, a normalization of the ultrasonic data was attempted based on the measured density and initial solids content determined for each of the three mixtures. The first component of the normalization was to multiply the UPV by the square root of the measured density of the concrete, since modulus is computed as density times UPV squared and strength is generally proportional to the square root of modulus (ACI 318, for example). For the solids content, the basic concept being explored is that the transmission speed of a sound wave depends on both its speed through the solid phases (related to their inherent stiffness/strength) and the volume of solid phases present. Thus, the quantity obtained by multiplying (1-air content)*(initial solids volume fraction) was used as the

second normalization factor for each mixture. In this factor, the air content was taken as the value estimated from the hardened cylinders after 1 d of sealed curing (assuming no mass loss during this curing, see Table 4) and the initial solids volume fraction included all solids present (cement, limestone powder, fine and coarse aggregate) with the exclusion of water and the HRWRA in the concrete mixture. While dividing the UPV values shown in the plot on the left side of Figure 25 by this normalization factor did bring the various curves closer together, dividing them by this normalization factor raised to the second power (squared) produced an almost perfect overlap for two of the three data sets. One hypothesis for why this normalization by the solids content raised to the second power works so well would be that the sound wave must propagate from one solid volume element to another to traverse the concrete specimen. Once the correlation length of the underlying microstructure is greatly exceeded, this probability of propagation (as characterized by the two-point correlation function) asymptotes to a value of the volume fraction squared [34,35]. While this normalization works well for two of the three concretes prepared with the same aggregates (and volume fractions), further research is necessary (and planned) to determine its universality across a wider range of concrete mixtures, including those prepared with different aggregate sources.

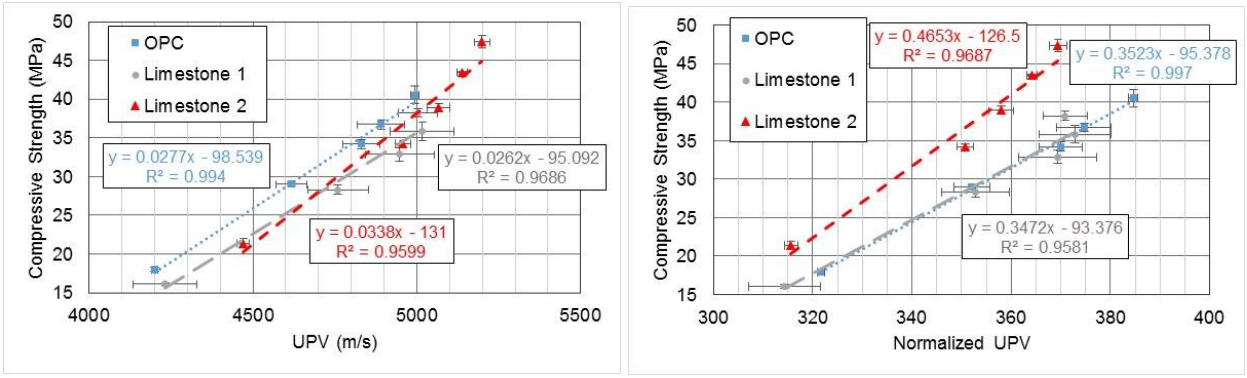

Figure 25. Cylinder compressive strength vs. measured (left) and normalized (right) UPV for the three concrete mixtures at ages of 1 d, 3 d, 7 d, 14 d, and 28 d (data points from left to right). Error bars indicate one standard deviation for measurements on three cylinders at each age for each mixture, except for the limestone 2 concrete mixture at the ages of 1 d and 3 d where five cylinders were tested and 7 d where four cylinders were tested.

Another approach to predicting concrete compressive strength is based on using its relation to cumulative heat release, as shown in Figure 26 (see also Figure 15 for corresponding results for mortars). This relation is typically limited to the first 7 d to 14 d of curing, as beyond this point, the signal to noise ratio for the measured heat release becomes too small for reliable data acquisition. However, out to 7 d, a linear relationship between cumulative heat release (normalized per unit mass of initial mixing water) and measured compressive strength is observed that is the same for two of the three concrete mixtures examined in the current study. As shown in Figure 26, the linear relationship found in this study for the OPC and limestone 1 concretes lies basically parallel to and between similar relationships found for two other aggregates (limestone and siliceous gravel) in previous studies [16,19], as the level of bond between the aggregates and the hydrating cement paste also influences strength, along with the porosity reduction produced by the cement hydration [7]. The dolomitic limestone (along with the siliceous sand) employed in the current study apparently produces a bond that is intermediate between that found in the limestone

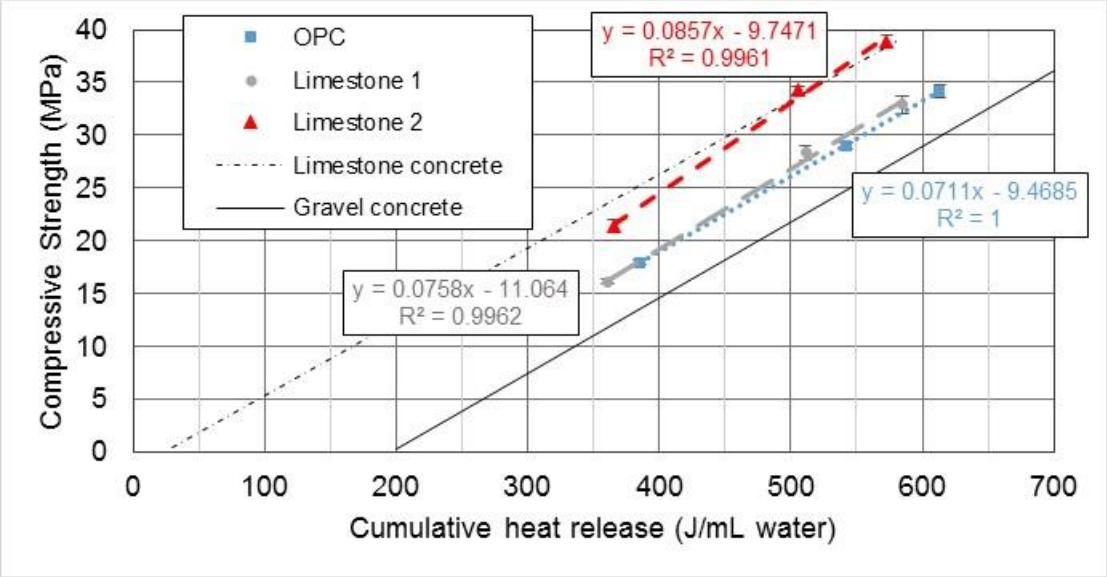

Figure 26. Cylinder compressive strength vs. measured cumulative heat release (from sieved mortar) for the three concrete mixtures at ages of 1 d, 3 d, and 7 d (data points from left to right). Dashed and thin solid lines indicate previously established relationships for limestone and gravel aggregate concretes, respectively [16,19].

(high bond) and gravel (low bond) concretes. However, with a higher limestone powder content and still less water (lower *w/s*), the line for the limestone 2 concrete mixture shifts upward to nearly match that of the previous limestone aggregate concrete, likely indicating a superior bonding between coarse aggregate and binder. Further support for a superior bond in the limestone 2 concrete mixture is provided in Figure 27 that contrasts split cylinder specimen (twin) surfaces (1 d breaks) for the OPC and limestone 2 concrete mixtures. The dark grey aggregates visible in each specimen generally correspond to aggregates that were fractured during the test, as can be verified by matching up the two pieces of each broken aggregate, one on each side of the broken specimen. There are far more of these broken aggregates present in the limestone 2 concrete mixture specimen, once again indicating a superior interfacial bond in this particular concrete.

The resistivity measurements for the three concrete mixtures at various ages are summarized in the graphs in Figure 28. At any given age (proceeding from left to right in the graph), the values measured for the OPC concrete generally lie between those measured for the two limestone concretes. As indicated in Table 6, this is the ordering that would be expected based on the estimated capillary porosity (Powers model) present in the three mixtures as a function of the degree of hydration of the cement (α) and the assumption that about 20 % capillary porosity in the paste is the volume fraction at which depercolation occurs [36,37]. Results obtained using either different devices to make uniaxial measurements or surface vs. uniaxial measurements are generally within 10 % to 20 % of one another, with the exception of the 28 d measurement of uniaxial resistivity of the limestone 2 mixture using device 1 that is abnormally high. Contributing factors to this could include the depercolation of the capillary porosity producing self-desiccation within these cylinder specimens and the lower measurement frequency (40 Hz) used with this device. One potential reason for a slightly greater difference between surface and uniaxial measurements (right side of Figure 28) than that found in a previous study [17] is that in the previous study, curing was conducted in a fog room, while in the present study, curing was

conducted in limewater where leaching of alkalis and other constituents from the surface of the concrete cylinders can impact particularly the measured surface resistivity [38,39]. Much less (if any) leaching would be expected under the standard fog room curing used in [17].

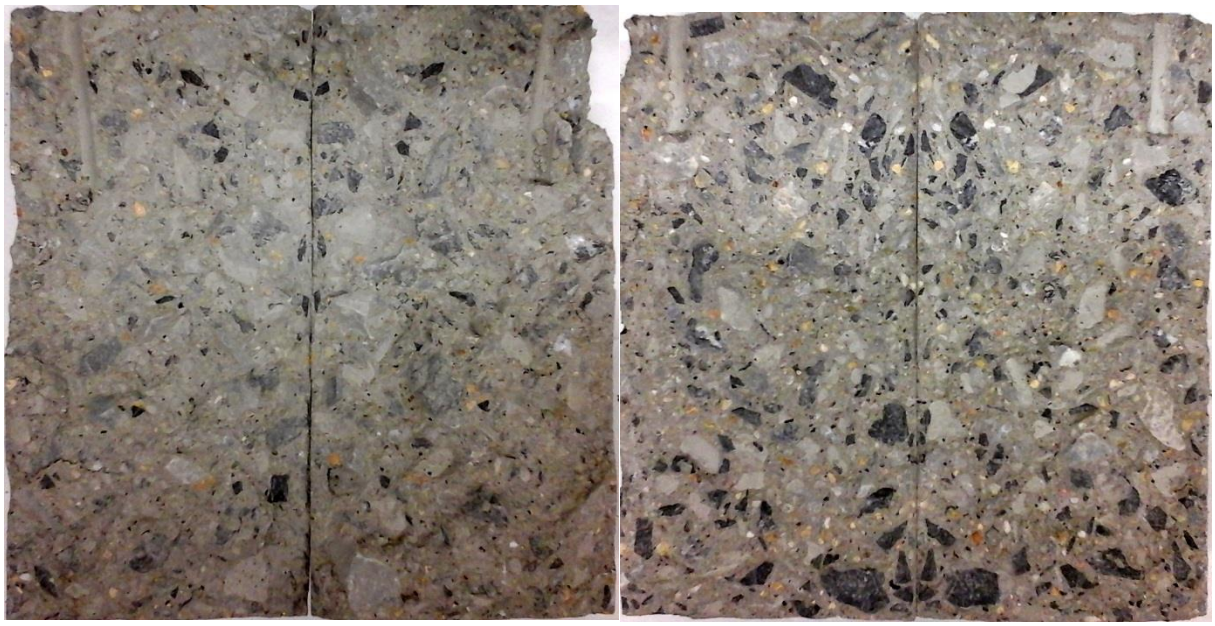

Figure 27. Photographs of specimen (twin) surfaces for OPC (left) and limestone 2 (right) concrete mixtures that were broken using a split cylinder test. Tube-shaped hole at top corner of each specimen corresponds to location of a plastic tube where a thermocouple was inserted. Dark grey aggregates in each case indicate fractured aggregates, as can be verified by matching them on the opposite side of the twin specimen. Each cylinder half is nominally 100 mm by 200 mm.

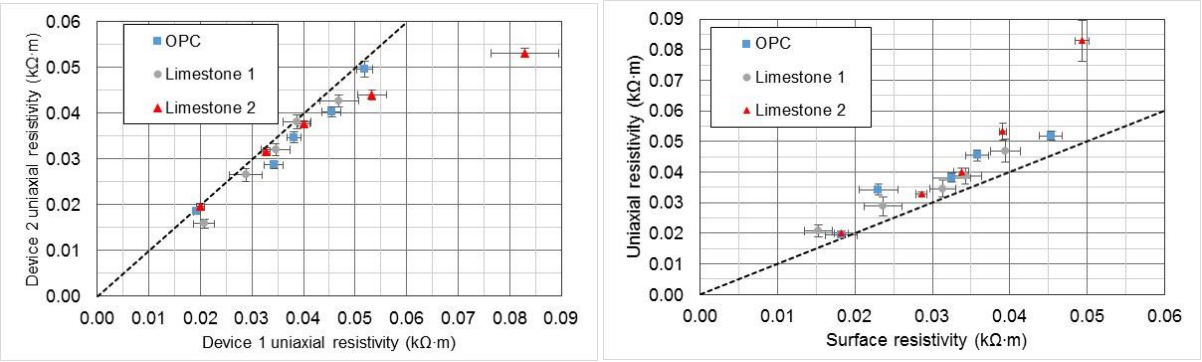

Figure 28. Comparison of uniaxial (left) resistivity measurements using two different measurement devices and uniaxial vs. surface resistivity (right) for the three concrete mixtures at ages of 1 d, 3 d, 7 d, 14 d, and 28 d (data points from left to right). Error bars indicate one standard deviation for measurements performed at each age for each mixture. The dashed line indicates a one-to-one relationship in each plot.

A comparison of concrete cylinder compressive strength plotted vs. the measured uniaxial resistivity (via device 2) is provided in Figure 29. For these three concrete mixtures, a single curve provides a reasonable representation of the relationship between strength and electrical resistivity,

either uniaxial or surface. However, once again, the strength values for the limestone 2 concrete mixture lie slightly above those of the other two concretes, further supporting its enhanced binder-aggregate bonding. While both electrical resistivity and compressive strength are largely influenced by the volume of capillary porosity within the hydrating cement paste component of the concrete, it is surprising that a single curve with some scatter is found to characterize fairly well the relationship between them for these concretes with quite different binder compositions. This would suggest that despite differences in binder composition, the impact of pore solution conductivity on measured electrical resistivity would be minimal; indeed, measurements of pore solution resistivity on the three mixtures have indicated values all within ± 20 % of 0.15 Ω·m, at ages of 1 d and beyond.

Table 6. Capillary porosity estimations for the paste components of the three concrete mixtures

Concrete	Porosity at α=0.85	α for 20 % porosity (depercolation)
OPC	23.4 %	0.926
Limestone 1	26.5 %	> 1.0
Limestone 2	21.4 %	0.893

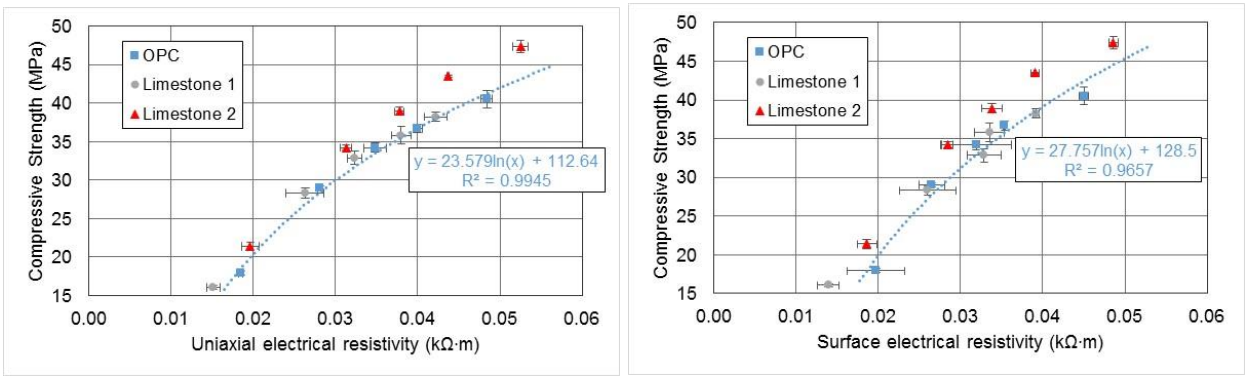

Figure 29. Measured compressive strength vs. uniaxial (left, measured at 10 kHz)) and surface (right) electrical resistivity for the three concrete mixtures at ages of 1 d, 3 d, 7 d, 14 d, and 28 d (data points from left to right). Error bars indicate one standard deviation for measurements on three cylinders at each age for each mixture, except for the limestone 2 concrete mixture at the ages of 1 d and 3 d where five cylinders were tested and 7 d where four cylinders were tested. Fitted line on each plot is for the OPC mixture only.

Summary

Studies in paste, mortar, and concrete have all confirmed the high potential for replacing a significant fraction of the cement paste in these materials with a fine limestone powder to produce more sustainable high volume limestone powder (HVLP) mixtures with equivalent or even superior performance. A key paradigm shift present in this approach is the concept of replacing cement paste (cement powder and water) with the limestone powder, as opposed to just replacing the cement powder. While particle packing can be optimized based on previously derived theoretical considerations [18], a fluid mixture generally requires moving away from any close-packed configuration, so that optimum packing is not paramount to obtaining acceptable performance in these systems.

Results in OPC and HVLP mortars indicated the viability of achieving cement reductions between 23 % and 38 %. In the mortar studies, the reduced autogenous and drying shrinkages of the HVLP mixtures were highlighted, being mainly due to their reduced paste content. In a series of three concretes, two HVLP concretes that provided 25.7 % and 27.7 % reductions in cement, respectively, performed similarly to the OPC reference mixture, with the second mixture actually offering a compressive strength boost on the order of 10 % to 20 % at ages to 28 d. With similar rheology (slump) and setting behaviors, these HVLP mixtures could be substituted for current OPC formulations, with minimal adjustments by the contractor and concrete construction crew being anticipated.

Although not the focus of the current study, the results for the three concrete mixtures have illustrated the strong relationships that exist between cumulative heat release, UPV, or electrical resistivity and measured compressive strength, which will be useful for developing noninvasive in situ measurements of in-place concrete compressive strength in an ongoing NIST exploratory research project. In this regard, a new approach to normalizing UPV data based on the solids contents of the concrete formulations was presented and partially verified using the data developed in this study. While isothermal calorimetry heat release is not easily monitored in the field (and certainly not in an in situ manner), UPV and (surface) electrical resistivity measurements can be easily adapted to the construction site and standardized for field deployment. One complication in using these techniques to predict strength that was highlighted in this study is their general inability to capture information concerning the binder-aggregate interfacial bond. In general, the limestone 2 concrete mixture, with a superior bond, did not follow the trends between these three measures and strength that were established for the first two concrete mixtures in this study. Further research on quantifying and improving the aggregate-binder bond in sustainable cement-based materials is needed and will be pursued by NIST in the future.

While the electrical resistivities measured on the concrete mixtures indicated a similar or superior performance for the HVLP mixtures in reference to the OPC mixture, further research will be needed to assure the durability of these higher replacement level sustainable concretes. Still, one encouraging fact is that concretes with up to 35 % limestone replacement for cement have been used for many years in parts of Europe with minimal durability concerns.

Acknowledgements

The authors would like to thank BASF, Carmeuse Lime and Stone, Huber Engineered Materials, the Lehigh Cement Company, OMYA Inc., U.S. Concrete, Inc., and W.R. Grace & Co.-Conn. for providing materials used in the present studies. The assistance of Mr. Max Peltz (NIST) in providing the measured particle size distributions, BET surface areas, and densities and assisting with the preparation of the mortar mixtures, Dr. Pan Feng (NIST) in obtaining the SEM/X-ray composite images of the powder blends, Ms. Lakesha Perry in conducting inductively coupled plasma atomic emission spectrometry (ICP-AES) measurements on pore solutions, Mr. Paul Rothfeld (NIST) in assisting with preparation of the mortar mixtures, Mr. Michael Boisclair (NIST) in performing data entry and analysis, and Mr. José David Betancourth Mendoza (UANL, Monterrey, MEXICO) in performing rheology measurements is gratefully acknowledged. The efforts of the following individuals (NIST) in assisting with the preparation and evaluation of the concrete mixtures is also greatly appreciated: Mr. Michael Boisclair, Mr. Richard Eason, Dr. Chiara Ferraris, Ms. Michelle Helsel, Mr. Max Peltz, and Mr. Paul Rothfeld.

References

1) Obla, K., Kim, H., and Lobo, C., "Effect of Continuous (Well-Graded) Combined Aggregate Grading on Concrete Performance, Phase B: Concrete Performance," NRMCA Research Laboratory Report, May 2007, available at: http://www.nrmca.org/research/D340%20AGR%20report%20phaseB.pdf .

2) Bentz, D.P., and Aïtcin, P.C., "The Hidden Meaning of Water-Cement Ratio: Distance between Cement Particles is Fundamental," *Concrete International*, Vol. 30 (5), 51-54, 2008.

3) Abrams, D.A., "Design of Concrete Mixtures," Bulletin No. 1, Structural Materials Research Laboratory, Lewis Institute, Chicago, 20 pp., 1918.

4) Bentz, D.P., Irassar, E.F., Bucher, B.E., and Weiss, W.J., "Limestone Fillers Conserve Cement Part 1: An Analysis Based on Powers' Model," *Concrete International*, Vol. 31 (11), 41-46, 2009.

5) Bentz, D.P., and Conway, J.T., "Computer Modeling of the Replacement of "Coarse" Cement Particles by Inert Fillers in Low *w/c* Ratio Concretes: Hydration and Strength," *Cement and Concrete Research*, Vol. 31, 503-506, 2001.

6) Li, L.G., and Kwan, A.K.H., "Adding Limestone Fines as Cementitious Paste Replacement to Improve Tensile Strength, Stiffness, and Durability of Concrete," *Cement and Concrete Composites*, Vol. 60, 17-24, 2015.

7) Bentz, D.P., Ardani, A., Barrett, T., Jones, S.Z., Lootens, D., Peltz, M.A., Sato, T., Stutzman, P.E., Tanesi, J., and Weiss, W.J., "Multi-Scale Investigation of the Performance of Limestone in Concrete," *Construction and Building Materials*, Vol. 75, 1-10, 2015.

8) Bentz, D.P., "Activation Energies of High-Volume Fly Ash Ternary Blends: Hydration and Setting," *Cement and Concrete Composites*, Vol. 53, 214-223, 2014.

9) ASTM Standards, Vol. 04.01, Cement; Lime; Gypsum, ASTM International, West Conshohocken, PA, 2014.

10) Gurney, L., Bentz, D.P., Sato, T., and Weiss, W.J., "Reducing Set Retardation in High Volume Fly Ash Mixtures with the Use of Limestone: Improving Constructability for Sustainability," *Transportation Research Record, Journal of the Transportation Research Board*, No. 2290, Concrete Materials 2012, 139-146, 2012.

11) AASHTO, "Standard Method of Test for Particle Size Analysis of Hydraulic Cement and Related Materials by Light Scattering," AASHTO T353-14-UL, 2014.

12) Bentz, D.P., Ferraris, C.F., Galler, M.A., Hansen, A.S., and Guynn, J.M., "Influence of Particle Size Distributions on Yield Stress and Viscosity of Cement-Fly Ash Pastes," *Cement and Concrete Research*, Vol. 42 (2), 404-409, 2012.

13) Bentz, D.P., and Ferraris, C.F., "Rheology and Setting of High Volume Fly Ash Mixtures," *Cement and Concrete Composites*, Vol. 32 (4), 265-270, 2010.

14) Bentz, D.P., Sant, G., and Weiss, J., "Early-Age Properties of Cement-Based Materials: I. Influence of Cement Fineness," *ASCE Journal of Materials in Civil Engineering*, Vol. 20 (7), 502-508, 2008.

15) ASTM Standards, Vol. 04.02, Concrete and Aggregates, ASTM International, West Conshohocken, PA, 2015.

16) Bentz, D.P., Tanesi, J., and Ardani, A., "Ternary Blends for Controlling Cost and Carbon Content," *Concrete International*, Vol. 35 (8), 51-59, 2013.

17) Bentz, D.P., Jones, S.Z., and Snyder, K.A., "Design and Performance of Ternary Blend High-Volume Fly Ash Concretes of Moderate Slump," *Construction and Building Materials*, Vol. 84, 409-415, 2015.

18) Brouwers, H.J.H., "Particle-size Distribution and Packing Fraction of Geometric Random Packings," *Physical Review E*, Vol. 74, 031309-1:14, 2006.

19) Bentz, D.P., Barrett, T. De la Varga, I., and Weiss, W.J., "Relating Compressive Strength to Heat Release in Mortars," *Advances in Civil Engineering Materials*, Vol. 1 (1), 14 pp., Sept. 2012.

20) Lootens, D., and Bentz, D.P., "On the Relation of Setting and Early-Age Strength Development to Porosity and Hydration in Cement-Based Materials," submitted to *Cement and Concrete Composites*, 2015.

21) Olivas, A., Ferraris, C.F., Guthrie, W.F., and Toman, B., "Re-Certification of SRM 2492: Bingham Paste Mixture for Rheological Measurements," NIST SP-260-182, August 2015.

22) Nkinamubanzi, P.-C., and Talbot, C., "Optimization of the Use of Ground Limestone in Concrete," Proceedings Thirteenth International Conference on Recent Advances in Concrete Technology and Sustainability Issues, Ottawa, Canada, July 2015.

23) Bullard, J.W., "MicroChar: An Application for Quantitative Analysis of Cement and Clinker Microstructure Images," NIST Technical Note **1876**, April 2015.

24) Bentz, D.P., Peltz, M.A., and Winpigler, J., "Early-Age Properties of Cement-Based Materials: II. Influence of Water-to-Cement Ratio," *ASCE Journal of Materials in Civil Engineering*, Vol. 21 (9), 512-517, 2009.

25) Bentz, D.P., Jensen, O.M., Hansen, K.K., Olesen, J.F., Stang, H., and Haecker, C.J., "Influence of Cement Particle Size Distribution on Early Age Autogenous Strains and Stresses in Cement-Based Materials," *Journal of the American Ceramic Society*, Vol. 84 (1), 129-135, 2001.

26) Lothenbach, B., Le Saout, G., Gallucci, E., and Scrivener, K., "Influence of Limestone on the Hydration of Portland Cements," *Cement and Concrete Research*, Vol. 38, 848-860, 2008.

27) Zajac, M., Rossberg, A., Le Saout, G., and Lothenbach, B., "Influence of Limestone and Anhydrite on the Hydration of Portland Cements," *Cement and Concrete Composites*, Vol. 46, 99-108, 2014.

28) Bentz, D.P., Jones, S.Z., Peltz, M.A., and Stutzman, P.E., "Influence of Internal Curing on the Properties and Performance on Repair Materials," NISTIR **8076**, U.S. Department of Commerce, July 2015.

29) Bentz, D.P., Stutzman, P.E., Sakulich, A., and Weiss, W.J., "Study of Early-Age Bridge Deck Cracking in Nevada and Wyoming," NISTIR **7841**, U.S. Department of Commerce, January 2012.

30) Bentz, D.P., and Peltz, M.A., "Reducing Thermal and Autogenous Shrinkage Contributions to Early-Age Cracking," *ACI Materials Journal*, Vol. 105 (4), 414-420, 2008.

31) Bentz, D.P., "Blending Different Fineness Cements to Engineer the Properties of Cement-Based Materials," *Magazine of Concrete Research*, Vol. 62 (5), 327-338, 2010.

32) Taylor, H.F.W., Cement Chemistry, 2nd edition, Thomas Telford, London, 1997.

33) CRC Handbook on Nondestructive Testing of Concrete, Eds. V.M. Malhotra and N.J. Carino, CRC Press, Boca Raton, 1991.

34) Bentz, D.P., "Three-Dimensional Computer Simulation of Portland Cement Hydration and Microstructure Development," *Journal of the American Ceramic Society*, Vol. 80 (1), 3-21, 1997.

35) Bentz, D.P., and Martys, N.S., "Hydraulic Radius and Transport in Reconstructed Model Three-Dimensional Porous Media," *Transport in Porous Media*, Vol. 17 (3), 221-238, 1995.

36) Bentz, D.P., and Garboczi, E.J., "Percolation of Phases in a Three-Dimensional Cement Paste Microstructural Model," *Cement and Concrete Research*, Vol. 21 (2), 325-344, 1991.

37) Snyder, K.A., and Bentz, D.P., "Suspended Hydration and Loss of Freezable Water in Cement Pastes Exposed to 90 % Relative Humidity," *Cement and Concrete Research*, Vol. 34 (11), 2045-2056, 2004.

38) Spragg, R.P., Villani, C., Weiss, J., Poursaee, A., Jones, S., Bentz, D.P., and Snyder, K.A., "Surface and Uniaxial Electrical Measurements on Layered Cementitious Composites having Cylindrical and Prismatic Geometries," in 4th International Conference on the Durability of Concrete Structures, Purdue University, West Lafayette, IN, July 24-26, 317-326, 2014.

39) Spragg, R., Bu, Y., Snyder, K., Bentz, D., and Weiss, J., "Electrical Testing of Cement-Based Materials: Role of Testing Techniques, Sample Conditioning, and Accelerated Curing," Publication FHWA/IN/JTRP-2013/28. Joint Transportation Research Program, Indiana Department of Transportation and Purdue University, West Lafayette, Indiana, 2013. doi: http://dx.doi.org/10.5703/1288284315230.